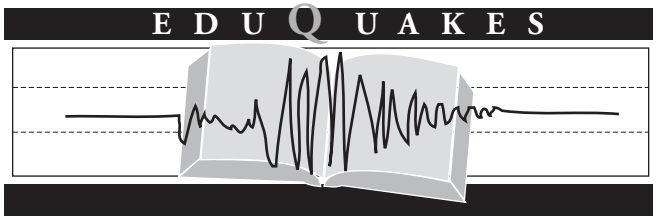

Student Guide: Making Waves by Visualizing Fourier Transformation

Robert Smalley, Jr.
Center for Earthquake Research and Information, The University of Memphis

Online material: Additional details of the mathematics.

INTRODUCTION

Using a simple graphical presentation we can visualize the integrand of the forward and inverse Fourier transforms as a topographic surface. This presentation aids in understanding frequency domain and real-space relationships, such as the important, but often poorly understood, contributiaon of the frequency domain phase spectrum to the real-space shape. The Fourier transform integrand visualization method presented here can also help develop insights into complex wave behavior, such as the relationship between traveling and standing waves and the evolution of dispersing wavetrains.

BACKGROUND

Fourier analysis is often introduced with a figure showing how to approximate a function by adding together sinusoids (Figure 1A). I extend this presentation through the introduction of Fourier transform integrand visualization (FTIV) and use this technique to illustrate the relationship between traveling and standing waves, the Fourier shift theorem, and how the phase affects the real-space shape of a dispersing wave.

Figure 1(A) shows a real space, in this case a time-domain function, a boxcar symmetric about $t = 0$, and the first few terms of its Fourier series

$$u(t) = \frac{c_0}{2} + \sum_{n=1}^{\infty}\left[c_n \cos(\omega_n t + \phi_n)\right], \quad \omega_n = n\omega_1, a_n \text{ real.} \tag{1}$$

The weights, $c(\omega_n)$, and phase shifts, (ϕ_n), represent u in the frequency domain. The cos $(\omega_n t)$ terms are known as basis functions and have variables from both domains, *i.e.*, time and frequency, in their argument. The set of basis functions must meet two important conditions. First, mutual orthogonality, which means you cannot make any of them by summing the others. Second, "completeness," which means any arbitrary function, with some conditions to ensure convergence, can be represented using only this set of functions. The Fourier series is also periodic, with period $T = 2\pi/\omega_1$.

The Fourier series can be generalized to the inverse Fourier transform

$$u(t) = \int_{-\infty}^{\infty} c(\omega)\cos(\omega t + \phi(\omega))\, d\omega \tag{2}$$

where the amplitude, $c(\omega)$, and phase, $\phi(\omega)$, spectra come from the Fourier transform

$$c(\omega) = \frac{1}{2\pi}\int_{-\infty}^{\infty} u(t)\cos(\omega t + \phi(\omega))\, dt \tag{3}$$

with $\phi(\omega)$ chosen to maximize $|c(\omega)|$. (The function $u(t)$ must be absolutely integrable and non-periodic.) The amplitude and phase spectra can be interpreted through the mathematical concept of correlation, which quantifies the similarity of functions; the Fourier transform is a correlation between the time-domain function and the time-shifted basis functions. The functions $u(t)$ and $F(\omega) = [c(\omega), \phi(\omega)]$ are known as a Fourier transform pair.

VISUALIZING THE FOURIER INTEGRAND

Relating frequency-domain and time-domain behaviors, especially those related to $\phi(\omega)$, is difficult with figures such as Figure 1(A), which typically use functions with $\phi(\omega) = 0$. FTIV illustrates the relationship between the Fourier transform pairs more clearly while naturally including $\phi(\omega)$. Figure 2(A) (shown on the back cover) introduces the FTIV technique using the basis functions of the forward and inverse Fourier transform integrands as a topographic surface. Figure 2(B) shows the inverse Fourier transform process; following the arrows, multiply the basis functions by $c(\omega)$ to make the inverse Fourier transform integrand, then integrate to obtain the boxcar. Figure 2(C) shows the process for the Fourier transform.

The $\phi(\omega)$ term in the basis function argument shifts the basis function's position along the real-space axis (step 0, Figure 2). This is the key to FTIV that allows showing both $c(\omega)$ and $\phi(\omega)$ in a clearly interpretable form. To examine the relationship between the time-domain shape and $\phi(\omega)$, consider a function with Fourier transform $c(\omega) = 1$, $\phi(\omega) = 0$. This makes a time-domain delta function at $t = 0$ (Figure 3). When $c(\omega) = 1$, contours of the inverse Fourier transform integrand amplitude are the same as contours of constant, or stationary, argument (we will hereafter refer to the basis function argument as the "phase"), and we will equate them. This relationship makes it

doi: 10.1785/gssrl.80.4.651

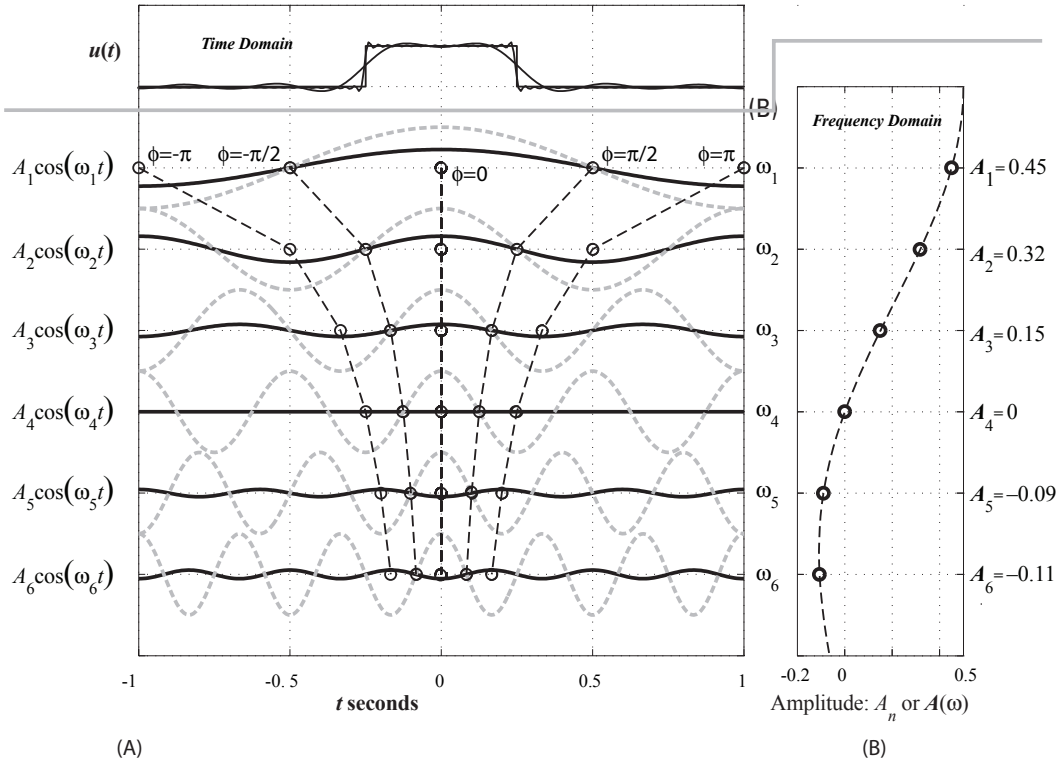

▲ **Figure 1.** (A) Time-domain boxcar approximations using 7 (heavy) and 100 (thin) Fourier series terms. First through sixth basis functions (gray dashed) and Fourier series terms (black). Points with stationary argument (circles) connected by vertical dashed lines between Fourier series terms become Fourier transform integrand lines of stationary phase. (B) Weights for Fourier series (circles) and Fourier transform (dashed line, scaled to match Fourier series).

easier to see the phase (*i.e.*, argument) behavior in Figures 2–5, which display the cosine of the phase and not the phase itself (a plot of the phase is not very illuminating).

The real-space function in Figure 3 is non-zero only at $t = 0$, where the phase is stationary. At $t = 0.49$, the phase varies linearly, and the integrand and running sum oscillate and remain small (zero). This observation is the basis of the principle of stationary phase: for functions that are oscillatory over most of their range, non-zero contributions to their integral come from integrand regions where the phase is stationary (*e.g.*, Udías 1999). We will refer to the contours seen in Figure 3 as skirts. Integrating along vertical paths, constructive/destructive interference occurs where the skirts are vertical/sloping.

EXAMPLES

Traveling Waves to Standing Waves and Back

Combining two sinusoidal waves traveling in opposite directions produces a standing wave (with k as "spatial frequency")

$$u(x,t) = \cos(kx + \omega t) + \cos(kx - \omega t) = 2\cos(kx)\cos(\omega t), \quad (k = 2\pi/\lambda \ , v = \omega/k \ ). \tag{4}$$

The right side of the equation shows a stationary wave in space, $\cos(kx)$, modulated in time by $\cos(\omega t)$. Now consider two deltas propagating at $\pm v$ (Figures 4A and 4B). The inverse Fourier transform integrands of traveling sinusoidal waves and time-domain deltas move to positions $x_1 = \pm v t_1$ at t_1. The real-space axis is now distance (distance-domain) and the real-space plot is a snapshot of the wavefield in space. Adding the wavefields of Figures 4(A)-ii and 4(B)-ii produces the wavefield in Figure 4(C)-ii. Alternately, adding the inverse Fourier transform integrands of traveling waves in Figure 4(A)-i and 4(B)-i produces an inverse Fourier transform integrand of standing waves in Figure 4(C)-i, which integrates to the traveling deltas in Figure 4(C)-ii. How do traveling waves arise from the integration of standing waves? The right side of Figure 4(C)-i shows the inverse Fourier transform integrand decomposed into the two standing wave factors, the $\cos(kx)$ component, from $x = 0$ to $x = 0.1$ (the delta's position), and the $\cos(\omega t)$ component, from $x = 0.1$ to $x = 0.25$. At $t = t_1$, the inverse Fourier transform is

$$u(x,t_1) = \int_{-\infty}^{\infty} \cos(\omega t_1)\cos(kx)\,dk \propto \delta(kx \pm \omega t_1) \ , \tag{5}$$

giving the traveling deltas at $x_1 = \pm\omega t_1/k = \pm v t_1$ from the orthogonality of the cosine. The $\cos(\omega t_1)$ term selects positions of $\cos(kx)$, which vary with time, having the same angular frequency forming a non-oscillatory integrand $\propto \cos^2(kx_1) = \cos^2(\omega t_1)$. At all other positions the integrand oscillates and integrates to zero.

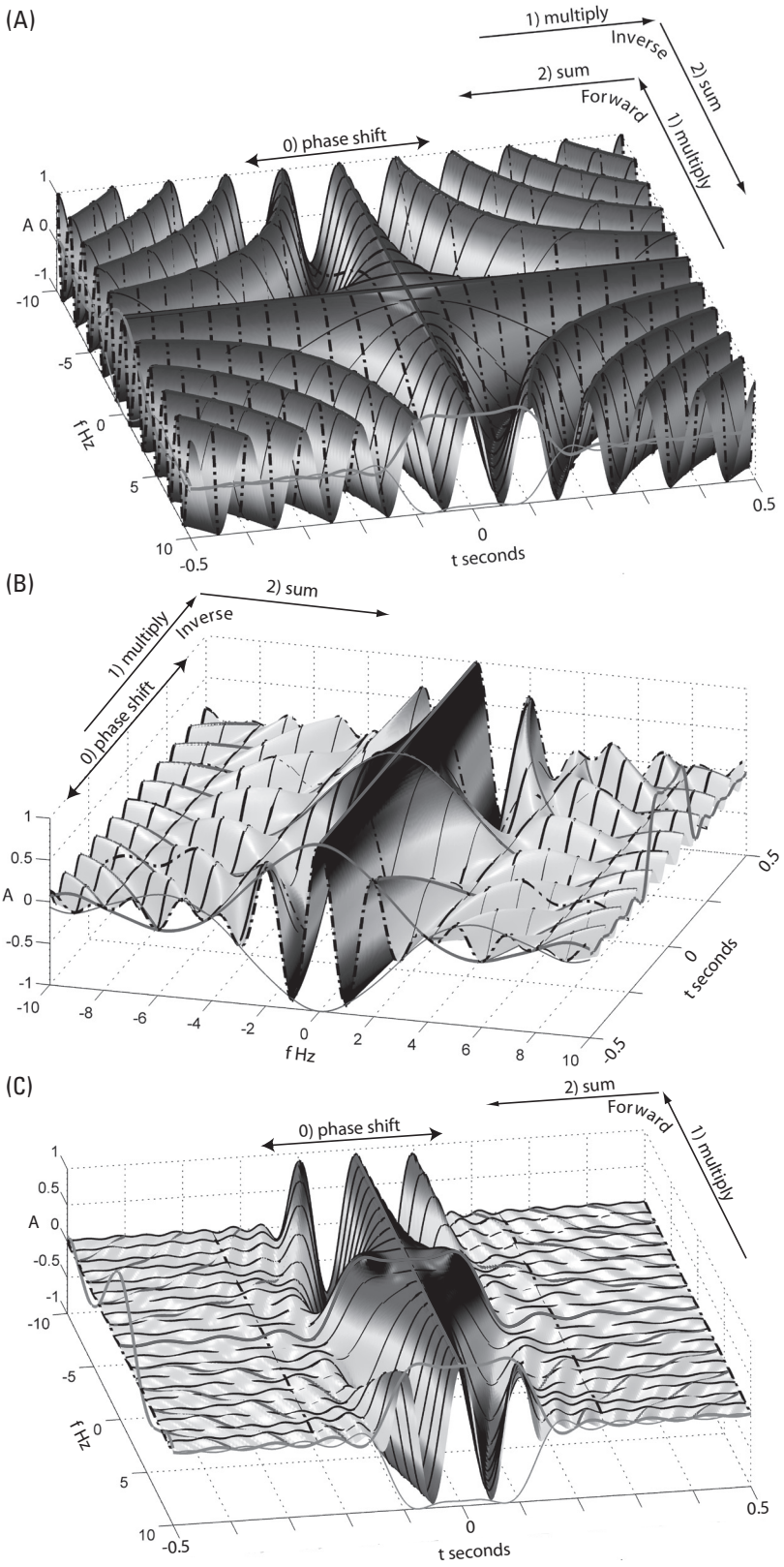

▲ **Figure 2.** (A) FTIV 3-D view of the common, basis function part of forward and inverse Fourier transform integrands as a surface. Frequency and time domain functions/envelopes (normalized to their maximum) shown by heavy/light plots along axes. Curves of constant amplitude and stationary phase shown on the back cover in blue. (B) Inverse Fourier transform integrand for boxcar after multiplying basis functions by $c(\omega)$. Sum parallel to f axis produces time-domain curve $u(t)$ along t axis. (C) Forward Fourier transform integrand for a boxcar after multiplying basis functions by $u(t)$. Sum parallel to t axis produces frequency-domain curve $C(\omega)$ along f axis.

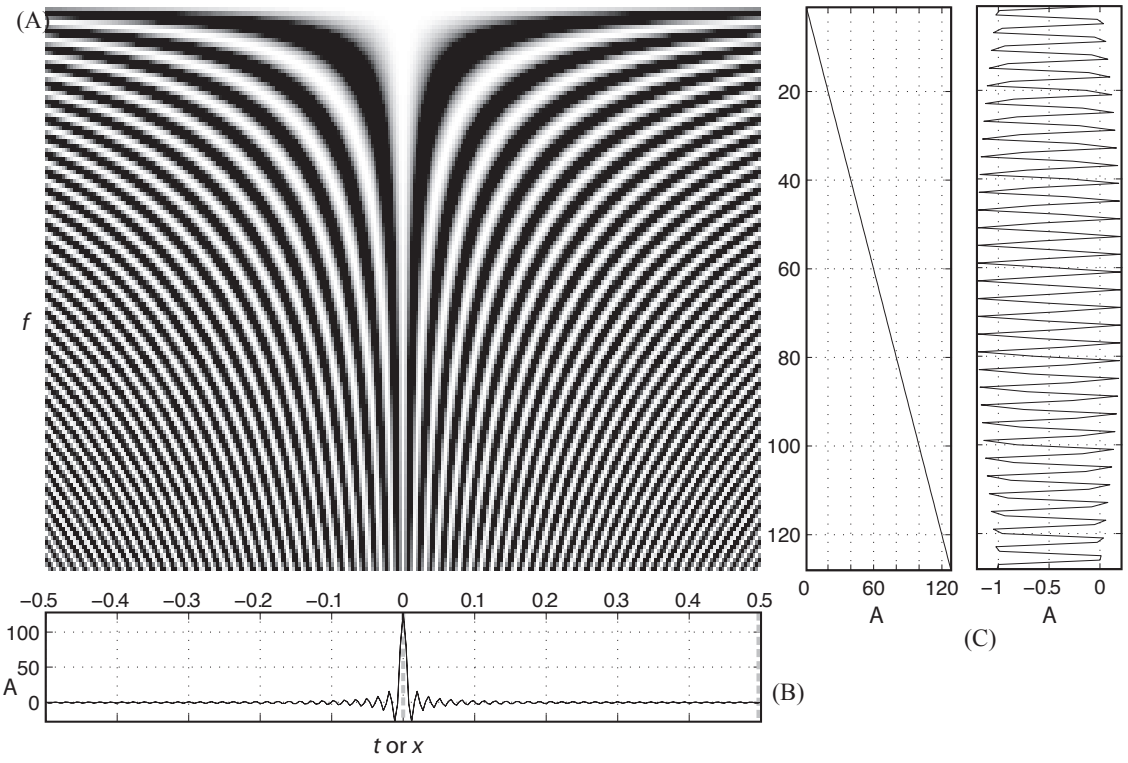

▲ **Figure 3.** FTIV gray scale topographic view of inverse Fourier transform integrand for a delta (top) with real-space function (bottom). Plots on right show running sums of the inverse Fourier transform integrand for profiles at two times or positions (gray dashed lines).

Fourier Shift Theorem

Shifting the delta also shifts the inverse Fourier transform integrand along the real-space axis (Figures 4A-i and 4B-i), providing a graphical view of the shift theorem: a real-space shift changes $\phi(k) \propto$ (real-space distance travelled/λ) $\propto kx$, but does not change $c(\omega)$.

Dispersion

When velocity is a function of frequency, $v(k)$, traveling waves change shape. Following Brune *et al.* (1960) and Nafe and Brune (1960), we now relate inverse Fourier transform integrand behavior to dispersion. Figure 5 (on the front cover) shows how, starting from the delta at $t = 0$, at t_1 each inverse Fourier transform integrand component traveled $x(k) = v(k)t_1$ to produce the inverse Fourier transform integrand (demonstrating how FTIV displays ϕ) and real-space wavefield shown. The vertical line of stationary phase at $x = 0, t = 0$ is sheared into a new shape (Figure 5A, see cyan line on front cover) and initially sloping inverse Fourier transform integrand skirts fold and go through vertical. The wavefield also evolved into a wide, complex shape in the region $v_3t_1 < x < v_1t_1$, which is wider than expected from the fast and slow velocity limits, $v_2t_1 < x < v_1t_1$. Where does the low velocity limit, v_3, come from? The answer is found by analyzing the skirt pattern.

Left of v_1 and right of v_3 the skirts slope, the integral is zero (Figure 5C-i, vi), and the real-space wave is not found. At v_1, the skirt is vertical for $0 < k < \alpha$, then slopes for $\alpha < k$. As regions with sloping skirts do not contribute to the integral, we can integrate over only $0 < k < \alpha$ to obtain $u(x, t) \propto \text{sinc}(X)\cos(k_0x - \omega_0t)$, $X \propto (x - v_1t)\delta k$, (Udías 1999). This is the product of a traveling sinusoidal carrier, $\cos(k_0x - \omega_0t)$, and a sinc modulation. The $(x - v_1t)$ term shifts the sinc's location by v_1t, while δk controls its width. A similar analysis can be done at v_2 for $\delta < k$. If the sinc is narrower than the sinusoids' wavelength the result looks like a sinc pulse ($x \approx -7.5$, Figure 5B-ii). If it is wider, the result looks like a sinusoidal wave with a sinc envelope ($x \approx 3.5$, Figure 5B-iv). The sinc envelopes move at v_1 or v_2 respectively, and restrict the wavefield to finite regions containing the wave's energy. The real-space wavefield comes from regions where the integrand's phase is stationary (Figure 5 C-ii and iv, gray background).

Between v_1 and v_2 the skirts fold. Here, waves with an observed k in the real-space wavefield, found by integrating the inverse Fourier transform integrand, do not travel at the $v(k)$ shown by the cyan curve. They are found to travel at a velocity defined by the magenta curve (Figure 5A). The magenta curve connects the set of points in the inverse Fourier transform integrand having stationary phase (vertical skirts) and defines a new type of velocity, the group velocity, $v_g(k)$, at which waves (and energy, etc.) travel in the real-space. The k and v observed at position x of the real-space wave (Figure 5B) are the same as those associated with the point of stationary phase, (x,k), on the magenta curve in the inverse Fourier transform integrand (Figure 5A). Figure 5 illustrates that phase velocity is easy to understand but hard to measure (nothing is physically traveling at the phase velocity), and that group velocity is hard to understand but easy to measure (it is the velocity of the physical wavefield we observe).

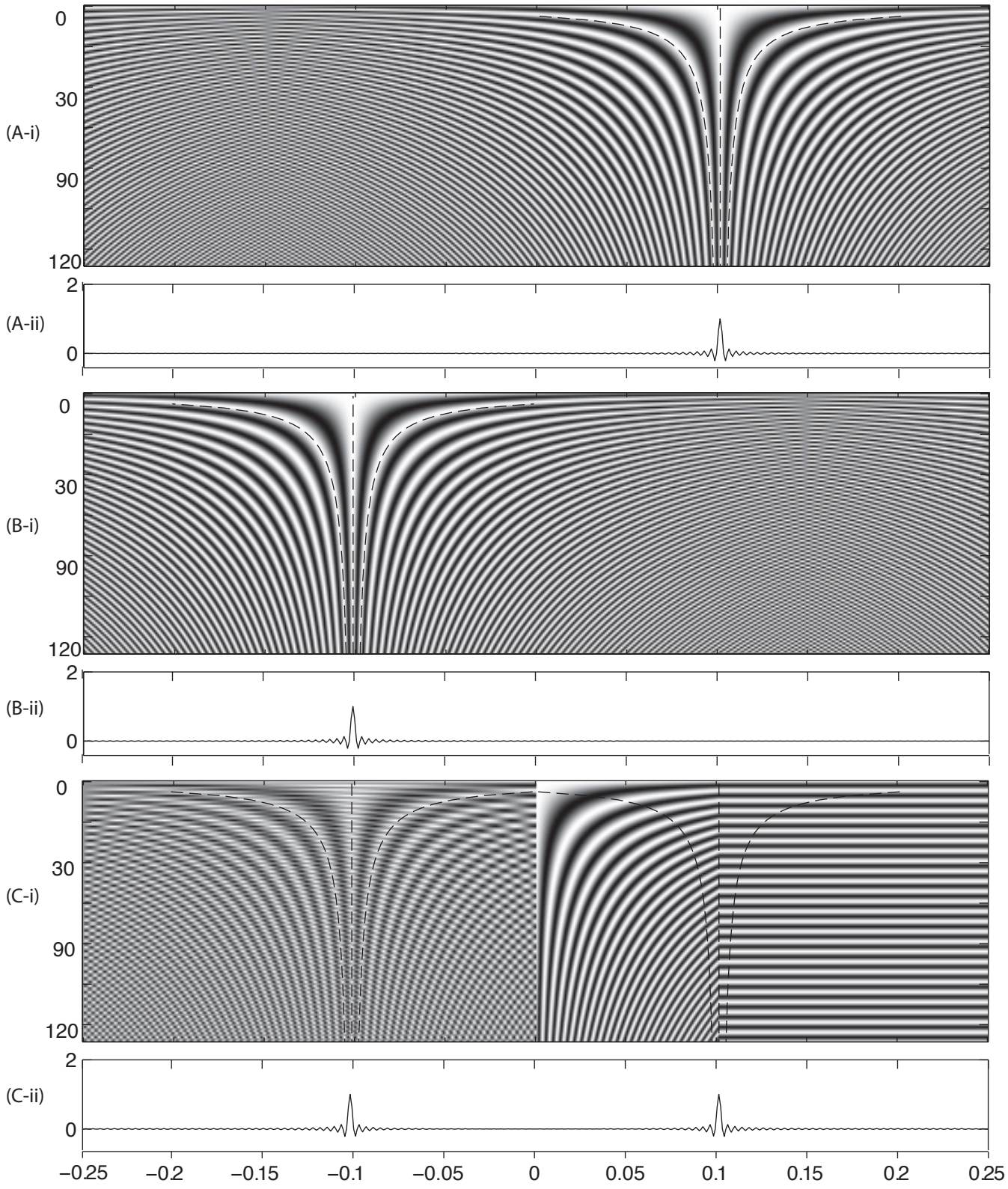

▲ **Figure 4.** Traveling waves in FTIV view of (A-i) and (B-i) combine into standing waves in the left side of (C-i). Solid and dashed curves in (A-i) and (B-i) show lines of stationary phase. These lines are also drawn in (C-i), where one sees a resemblance of the skirt patterns. Right side of (C-i) shows product form: a fixed spatial delta, $\cos(kx)$, modulated by $\cos(\omega x)$. Real-space traveling deltas from integration if inverse Fourier transform integrands are shown in (A-ii), (B-ii) and (C-ii).

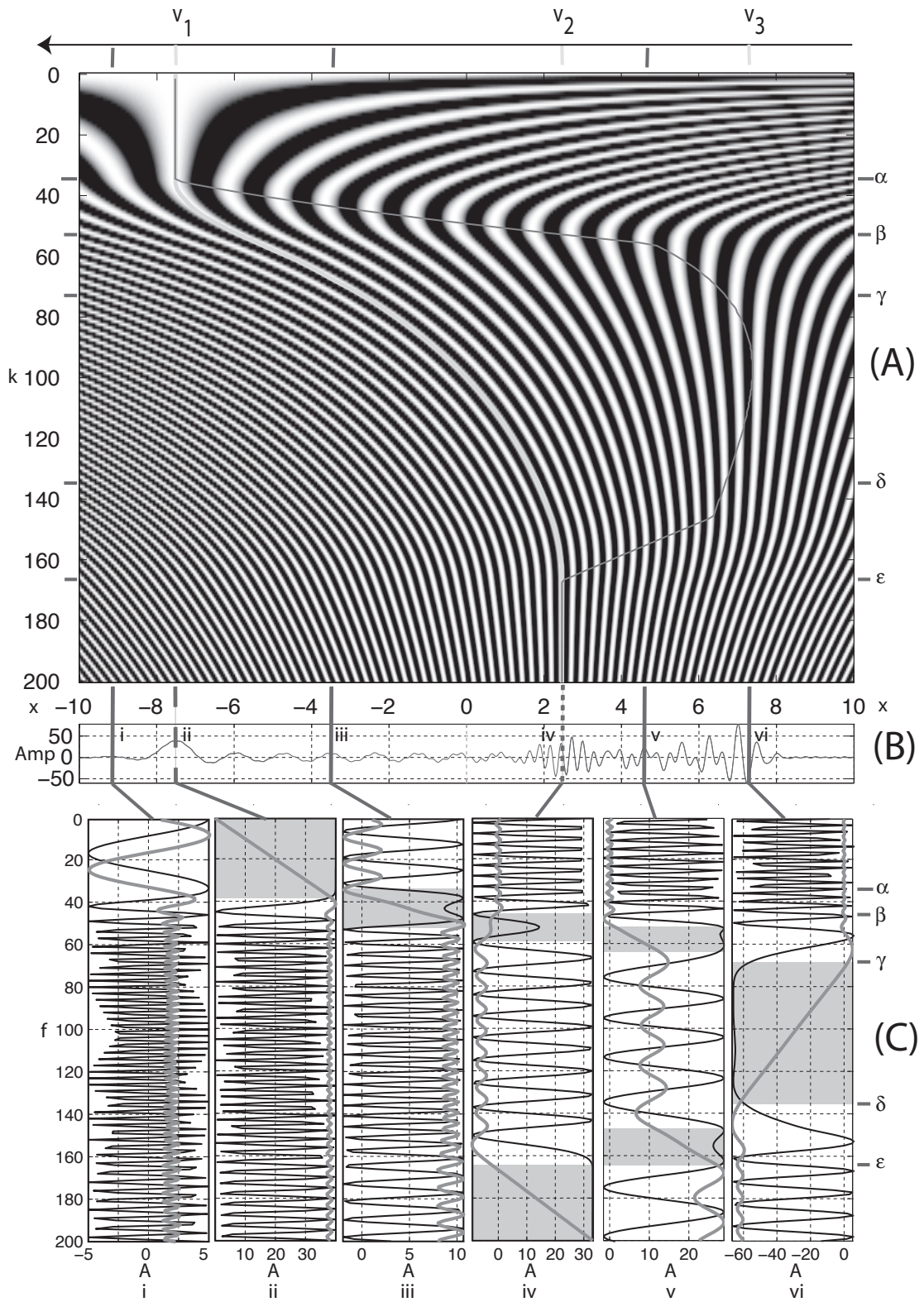

▲ **Figure 5.** Illustration of dispersion, phase and group velocities, and principle of stationary phase. (A) Inverse Fourier transform integrand ($\cos(kx - \omega(k)t)$, $v(k) = \omega(k)/k$) and (B) plot of dispersed wave. The distance axis, shared by inverse Fourier transform integrand and real-space plots, pans with the wave. Rescaling the x axis by $1/t_1$ changes it to velocity (top) with phase and group velocities shown by cyan and magenta curves on the front cover. Yellow ticks on v axis mark fast and slow limits of phase and group velocities. (C) Inverse Fourier transform integrand profiles (black, scale ±1) and running sums (red, i through vi, scale labeled). Ticks on k axis (A and C, right side) mark frequency bands for classes of real-space behavior associated with regions of stationary phase (gray background).

The inverse Fourier transform integrand skirt pattern, real-space shape, and group velocity are related by the principle of stationary phase, which applies to integrating the product of a slowly varying function and a rapidly oscillating function (see Båth 1968). In our case, the slowly varying function is $c(k) = 1$, and we only have to consider the oscillatory term, $\cos(kx - \omega(k)t)$, greatly simplifying the discussion without losing insight. When the phase is stationary (constant, vertical skirt),

$$\begin{aligned} (kx - \omega(k)t) &= \Psi(k,x) = C, \\ \partial\Psi/\partial k\big|_x &= 0, \\ x/t &= d\omega(k)/dk\big|_x = U(k). \end{aligned} \tag{6}$$

The contribution to the wavefield from Fourier component k arrives at x at velocity $v_g = U(k)$. A branch of stationary phase is found between $v_2 t_1 < x < v_1 t_1$ in $\alpha < k < \beta$, producing a sinusoidal wavefield of slowly decreasing wavelength. A running sum (Figure 5C-iii) shows that the largest contribution to the wavefield comes from the small region (x, k) (gray background) of the skirt pattern fold where the phase is stationary. There are two stationary phase branches in $v_3 t_1 < x < v_2 t_1$, $\beta < k < \gamma$ and $\delta < k < \varepsilon$, and the non-zero contributions come from the two stationary phase regions (Figure 5C-v).

Finally, v_3 is an inflection point where the second derivative of the phase is also zero, indicated by the vertical skirt in $\gamma < k < \delta$ that does not form a closed fold. Using an extension of the principle of stationary phase, we obtain a large amplitude pulse known as the Airy phase, associated with an extremum (minimum) of the group velocity (Figure 5C-vi).

DISCUSSION AND CONCLUSIONS

We have seen that $\phi(\omega)$ can have significant effects on the real-space shape. How does this compare to the effects of $c(\omega)$? The shape of the boxcar comes from $c(\omega)$. We saw that a delta with $c(\omega) = 1$ and $\phi(\omega) = 0$ can generate a dispersed seismogram through variation of only the phase spectrum. For $c(\omega) = 1$ and random phase, the time-domain function is white noise. The delta, white noise, and dispersed wavetrain all have $c(\omega) = 1$, but different real-space functions determined by $\phi(\omega)$, which shows that the phase spectrum carries important information and can be a major contributor to the real-space shape and its time evolution. The shape of a wave as it propagates depends on changes in both $c(\omega)$ and $\phi(\omega)$. Viewing the forward and inverse Fourier transform integrands as a topographic surface provides insight into a number of real-space wavefield features such as the often underappreciated phase spectrum contribution to the real-space function, how to make traveling waves from standing waves, and the behavior of dispersing wavefields.

ACKNOWLEDGMENTS

I thank C. Langston, J. Pujol, M. Bevis, and *SRL* Editor L. Astiz for helpful reviews.

REFERENCES

Båth, M. (1968). *Mathematical Aspects of Seismology.* Developments in Solid Earth Geophysics 4. New York: Elsevier, 415 pps.

Brune, J. N., J. E. Nafe, and J. E. Oliver (1960). A simplified method for the analysis and synthesis of dispersed wave trains. *Journal of Geophysical Research* **65** (1), 287–304.

Nafe, J. E., and J. N. Brune (1960). Observations of phase velocity for Rayleigh waves in the period range 100 to 400 seconds. *Bulletin of the Seismological Society of America* **50** (3), 427–439.

Udías, A. (1999). *Principles of Seismology*. Cambridge: Cambridge Univ. Press, 475 pps.

Center for Earthquake Research and Information
University of Memphis
Memphis, Tennessee 38152 U.S.A.
smalley@ceri.mempis.edu

Electronic supplement to

Student Guide: Making Waves by Visualizing Fourier Transformation

By Robert Smalley, Jr.

EduQuakes column from *Seismological Research Letters* Volume 80, Number 4 July/August 2009

Introduction

The Fourier transform integrand visualization (FTIV) method introduced here is based on a simple graphical presentation of the Fourier transform integrand as a topographic surface. FTIV is useful for understanding the important but often underappreciated contribution of the frequency-domain representation's phase spectrum to the shape of the function in the real-space. As the frequency-domain is the natural space for describing waves, this approach can also be used to develop insights into complex wave behavior, such as the relationship between traveling and standing waves and the evolution of the shape of a dispersing wave-train.

Figures 1-4 are the same as the figures in the printed version. Figure 5 in this e-supplement is a modified version of Figure 5 in the printed version. Figures 6 and 7 in this e-supplement are in addition to those in the printed version. The equations are numbered such that the whole number equations in red are the same as in the printed version. Additional equations that are only in this e-supplement are numbered with decimal values that count equations between those in the printed version.

Background

Introductory physics and engineering textbooks, which typically encourage visualization, often start their discussion of Fourier analysis with a figure showing how one can approximate a function in some real-space by adding together sinusoids in an appropriate frequency-domain (Figure 1(A)). The introduction of Fourier analysis is also oftentimes associated with solutions to differential equations; especially the wave equation for which sinusoids are also solutions. In this case, a relationship between the Fourier representation, which otherwise seems arbitrary, and the physics of the problem is established, allowing one to relate the two and provide insights into the physics. We will use examples with traveling and standing waves to show how a graphical presentation can illustrate fundamental ideas such as the shift theorem, superposition and stationary phase and how they affect the time-domain shape.

In the typical introduction, the real-space is usually time or space (distance), and we will use the terms time-domain or distance-domain as appropriate to refer to them. Figure 1(A) shows a time-domain function, in this case a "boxcar" centered at $t = 0$ and the first few terms of the Fourier series that approximates it

$$u(t) = \frac{a_0}{2} + \sum_{n=1}^{\infty}\left[a_n \cos\left(\omega_n t\right)\right], \quad \omega_n = n\,\omega_1, a_0 \text{ and } a_n \text{ real} \qquad (0.1)$$

(we will clarify the ω_1 term below, for $n = 0$, $\omega_0 = 0 \times \omega_1 = 0$ and $\cos\left(\omega_0\, t\right) = 1$, so the a_0 term is just a DC shift and treated separately). This is not the most general (it can only represent symmetric functions for example) or elegant form of the Fourier series, but it allows a graphical illustration that presents the fundamental ideas. The frequency-domain representation of the boxcar is the set of weights, a_n, used in the Fourier series sum. Figure 1(A) also shows the time-domain approximation obtained from summing a larger number of terms in the Fourier series. Note that the final sum, $u(t)$, is in the time-domain only, i.e. it is a function of time only, while the frequency-domain representation is the series of weights, a_n, associated with frequency only. The functions, $\cos\left(\omega_n t\right)$, in Eq. (0.1) are known as basis functions, and they have both time and frequency in their argument. We will use the term phase to refer to their arguments. The set of basis functions can be used in a Fourier series to generate any other function. The basis functions need to have two important properties. First they must be mutually orthogonal (perpendicular), which means you cannot make any of the basis functions from a sum of the others. This is expressed mathematically as

$$\int_{-\infty}^{\infty} \cos\left(\omega_n t\right)\cos\left(\omega_m t\right) dt = \delta\left(n - m\right) \qquad (0.2),$$

where $\cos\left(\omega_n t\right)$ and $\cos\left(\omega_m t\right)$ are the n^{th} and m^{th} basis functions and $\delta(n-m)$ is known as the delta function and is defined as

$$\delta(x) = \begin{cases} 1 & x = 0 \\ 0 & x \neq 0 \end{cases}, \qquad (0.3)$$

where $x = n - m$ in this case. The set of basis functions must also have the property that they are "complete". This means that any arbitrary function, meeting some general conditions to ensure the Fourier series converges, can be represented using only this set of functions. While Figure 1(A) suggests the Fourier series represents a single boxcar, the Fourier series is actually periodic (more precisely, the Fourier series is only applicable to periodic functions), with the period based on ω_1. If we plotted $u(t)$ for a range of t larger than that shown in Figure 1(A) we would see this periodicity as a repetition of the boxcar every mT, where $T = 2\pi/\omega_1$ is the period and m is an integer. Note that the function u is continuous in the time-domain, but its representation in the frequency-domain is discrete.

The general form of the Fourier series, which can represent arbitrary periodic functions is,

$$u(t) = \frac{a_0}{2} + \sum_{n=1}^{\infty} \left[\; a_n \cos\left(\omega_n t\right) + b_n \sin\left(\omega_n t\right) \;\right]. \qquad (0.4)$$

This can be written as

$$u(t) = \frac{a_0}{2} + \sum_{n=1}^{\infty} c_n \cos\left(\omega_n t + \phi_n\right). \quad (1)$$

This form will facilitate making the FTIV figures. The a_n, b_n and c_n are all real with

$$c_n = \sqrt{a_n^2 + b_n^2} \qquad (1.1)$$

and the phase value associated with the n^{th} or ω_n term is

$$\phi_n = -\tan^{-1}\left(\frac{b_n}{a_n}\right). \qquad (1.2)$$

The ϕ_n term provides a constant phase shift in the argument $\left(\omega_n t + \phi_n\right)$ of the basis function in Eq. (1). Note the distinction between the phase argument of the basis function, the expression $\left(\omega_n t + \phi_n\right)$, and the phase value, ϕ_n, which is part of the phase argument.

The elegant form of the Fourier series is

$$u(t) = \sum_{n=-\infty}^{\infty} F_n \; e^{i\,\omega_n t}, \qquad (1.3)$$

which, with $F_n = c_n\, e^{i\phi_n}$, can be written

$$u(t) = \sum_{n=-\infty}^{\infty} c_n\, e^{i\phi_n} \; e^{i\omega_n t} = \sum_{n=-\infty}^{\infty} c_n \; e^{i\left(\omega_n t + \phi_n\right)}. \qquad (1.4)$$

(We will use lower case letters for real, and upper case letters for complex values or functions.).

The forms in Eq. (0.4) and Eq. (1.3) are the forms that are usually presented. They are difficult to use for graphical presentations, however, as they have two parts (the weights for both the sines and cosines, or the magnitudes and phase values for the complex exponential) that cannot be combined in a single illustrative figure. This is one reason why the boxcar was chosen for Figure 1; it is symmetric about zero making $\phi_n = 0$. We will find the form in Eq. (1), however, to be very useful in for making the FTIV figures since the phase value, ϕ_n, simply shifts or moves the position of the cosine wave along the t axis. This allows the full frequency-domain representation to be shown in terms of its amplitude and phase in a clearly interpretable form in the FTIV figures.

The discrete sum of the Fourier series can be generalized to the continuous inverse Fourier transform given by

$$u(t) = \int_{-\infty}^{\infty} F(\omega)\ e^{i\omega t} d\omega\ , \qquad (1.5)$$

where the weighting function

$$F(\omega) = a(\omega)\ e^{i\phi(\omega)} \qquad (1.6)$$

is known as the Fourier transform and is the frequency-domain representation of $u(t)$. $F(\omega)$ is a continuous function of ω only, and is complex with a magnitude, $a(\omega)$, known as the amplitude spectrum, and phase, $\phi(\omega)$, known as the phase spectrum. The functions $u(t)$ and $F(\omega)$ are known as a Fourier transform pair, expressed as

$$u(t) \leftrightarrow F(\omega), \qquad (1.7)$$

and represent the same function specified in the two domains. While there are some additional conditions on the time-domain function to ensure that the Fourier transform integral is well behaved, the Fourier transform is restricted to absolutely integrable, non-periodic functions.

Following Eq. (1), it is more useful for FTIV to write the inverse Fourier transform as

$$u(t) = \int_{-\infty}^{\infty} c(\omega)\ \cos\left(\omega t + \phi(\omega)\right)\ d\omega\ , \qquad (2)$$

where the phase spectrum component, $e^{i\phi(\omega)}$, of the Fourier transform is combined with the basis function component, $e^{i\omega t}$.

Given the weights for the Fourier series, it is easy to show how the summation begins to look like the boxcar after summing just a few terms, and the typical mental pictures of the Fourier series and the inverse Fourier transform are based on the idea of summation. How does one obtain the Fourier transform weights, a_n, b_n, or $F(\omega_n)$ for the Fourier series, or the function, $F(\omega)$, for the inverse Fourier transform? Using the form of the Fourier series in Eq. (1), and ignoring the $a_0/2$ term (which will go away upon integration for $m \neq 0$), consider

$$\int_{-\infty}^{\infty} u(t)\cos\left(\omega_m t\right) dt = \qquad (2.1)$$

$$\int_{-\infty}^{\infty} \left(\sum_{n=1}^{\infty} \left[a_n \cos\left(\omega_n t\right) + b_n \sin\left(\omega_n t\right) \right] \right) \cos\left(\omega_m t\right) dt = a_n \delta(n-m)\,.$$

We arrive at this result by changing the order of integration and summation and using the orthogonality of the basis functions given in Eqs. (0.2) and (0.3). In the standard form for the Fourier series weights we have

$$a_n = \frac{1}{2\pi} \int_{-\infty}^{\infty} u(t) \cos(\omega_n t) \, dt \ , \qquad (2.2)$$

$$b_n = \frac{1}{2\pi} \int_{-\infty}^{\infty} u(t) \sin(\omega_n t) \, dt \ , \qquad (2.3)$$

and for the more elegant form,

$$F(\omega_n) = \frac{1}{2\pi} \int_{-\infty}^{\infty} u(t) \, e^{-i\omega_n t} dt \ . \qquad (2.4)$$

We can interpret the weights by turning to the mathematical concept of correlation, which, in this context, provides a measure of the similarity of two functions. The general expression for the correlation between the functions $g(t)$ and $h(t)$ is

$$\int_{-\infty}^{\infty} g(t) h(t) dt \, . \qquad (2.5)$$

If the two functions are the same, the correlation will be a maximum. If they are negatives of one another, the correlation will be the same magnitude but negative. For functions that are not the same, the correlation varies between these two limits and has a minimum magnitude of zero for two functions that are completely uncorrelated (two different Fourier basis functions for example). The expressions in Eq. (2.2-2.4) are correlations that quantify how similar the time-domain function, $u(t)$, is to each of the basis functions.

As with the Fourier series, we will find it helpful to use the form

$$c_n = \frac{1}{2\pi} \int_{-\infty}^{\infty} u(t) \cos(\omega_n t + \phi_n) \, dt \ , \qquad (2.6)$$

where c_n is the Fourier series weight and ϕ_n is the phase value in Eq. (1.2), and these terms give the amplitude and phase spectra respectively. This is a form of the correlation function

$$q(t) = \int_{-\infty}^{\infty} g(\tau) h(\tau + t) d\tau \, , \qquad (2.7)$$

which finds the correlation between the functions as a function of a shift, t. The value of c_n and ϕ_n are found from the maximum of the correlation function as a function of ϕ

$$(c_n, \phi_n) = \max_{0 \le \phi < 2\pi} \left(\frac{1}{2\pi} \int_{-\infty}^{\infty} u(t) \cos(\omega_n t + \phi) \, dt \right). \qquad (2.8)$$

Conceptually, the c_n and ϕ_n are found together by searching over values of ϕ, which simply shifts the cosine basis function back and forth along the time axis, to find the maximum value of the integral (correlation) for c_n. Due to the periodicity of the cosine

function, we only have to examine phase shifts over a range of 2π (for periodic signals the resulting correlation is also periodic, and there is no single shift for maximum correlation). In practice, we can use the standard forms in Eqs. (2.2) and (2.3) to calculate the weights, and then use Eqs. (1.1) and (1.2) to calculate the c_n and ϕ_n. We could also evaluate the correlation function (which can be done easily in the frequency-domain) and choose its maximum value and the associated shift. The weights in the frequency-domain are therefore proportional to how correlated or similar the time-domain function and the shifted basis functions are. We now have two values associated with each frequency, ω_n; the weight, also called the magnitude, c_n, and a phase shift, ϕ_n, that are easily interpreted both physically and in the figures of the FTIV method.

To find the Fourier transform, $F(\omega)$, the expression for the Fourier series weights in Eq. (2.6), can be generalized to

$$F(\omega) = \frac{1}{2\pi} \int_{-\infty}^{\infty} u(t)\ e^{-i\omega t} d\omega\ , \qquad (2.9)$$

which is also a correlation between $u(t)$ and $e^{-i\omega t}$, although it is difficult to visualize and is not usually presented as such. Following the treatment of the Fourier series, with $F(\omega) = c(\omega)\ e^{i\phi(\omega)}$, we can write

$$c(\omega) = \int_{-\infty}^{\infty} u(t)\cos\left(\omega t + \phi(\omega)\right) dt\ , \qquad (3)$$

where, as is the case with the Fourier series, $\phi(\omega)$ is determined such that $|c(\omega)|$ is a maximum.

Note that the naming of the various Fourier entities is not consistent, and there are several arbitrary choices in the definitions. The Fourier series and inverse Fourier transform produce the time-domain representation from the frequency-domain representation, while the Fourier transform, or forward Fourier transform, produces the frequency-domain representation from the time-domain representation. There is no general name for the expression to generate the weights of the Fourier series, Eqs. (2.2-2.4, 2.6), nor is there an inverse Fourier series. The signs of the exponential factors in Eqs. (1.5) and (2 .9) must be the negatives of one another, but the selection of the sign is otherwise arbitrary. The $1/2\pi$ scaling factor may also be placed in the definition of the inverse Fourier transform Eq. (1.5) rather than Eq. (2.9), placed symmetrically on both the forward and inverse transforms as $1/\sqrt{2\pi}$, or done away with altogether by a variable substitution $f_n = 2\pi\omega_n$. Mathematicians, physical scientists, and engineers each prefer a different convention. In general, in this tutorial presentation, we will concentrate on the functional forms and graphics and not show the scaling factors.

Fourier Transform Integrand Visualization

It is difficult, unfortunately, to illustrate many interesting properties of the

relationship between the frequency-domain and time-domain behaviors, especially those related to the phase spectrum, using figures such as Figure 1(A). The vertical axis in the bottom portion of Figure 1(A), represents frequency as one goes between the labeled, horizontal frequency axes. For the plot of each weighted sinusoidal component, shown in black, however, the individual vertical axes represent amplitude for that component. The change in amplitude and sign of the sinusoidal terms is due to the Fourier weighting for a boxcar, which is shown in Figure 1(B) for both the continuous Fourier transform (green curve) and the Fourier series (green circles). In Figure 1(B), the values shown for the Fourier transform and Fourier series have been scaled to make the two plots overlay one another, illustrating they are the same function (almost: the Fourier series is periodic and the Fourier transform is a single boxcar). A number of blue circles are also shown in the lower part of Figure 1(A) that define lines in (t,ω) where the argument to the sinusoid, and, therefore, the value of the sinusoid, is constant. The lines connecting these points are known as lines of constant phase. The argument to the sinusoidal basis function, the phase, is the same along each of them. We will return to these lines later and see that they are important in understanding the shape of the time-domain function.

FTIV can be used to provide a view of the frequency and time-domain Fourier pairs that more clearly illustrates the relationship between the frequency and time-domain representations of a function. In Figure 2(A), we show the basis function component of the integrand for both the forward and inverse Fourier transforms as a surface in (t,ω) space that is formed by draping an "altitude" color-coding over an illuminated 3-D view of the topography,

$$z(t,\omega)=\cos(\omega t). \qquad (3.1)$$

The application of lighting and shading helps the brain visualize the surface. Sums over frequency, i.e., sums along lines parallel to the frequency axis in Figure 2(B),

$$u(t_m)=\sum_{n=1}^{n_{\max}} c_n \cos(\omega_n t_m), \qquad (3.2)$$

generate the inverse Fourier transform and produce the time-domain function also shown in Figure 2(B). Note that we cannot do continuous math on the computer and, therefore, simulate the continuum by taking dense, discrete samplings in both ω and t. Integration over ω is replaced by summing over this dense sampling. The additional discretization in time will introduce additional properties and limitations to the application of Fourier analysis, specifically a maximum frequency related to the time step and a periodicity in the frequency-domain with respect to this maximum frequency. While the differences between continuous math and discrete math are interesting and important, and have to be taken into account when producing the figures, they will complicate the current discussion, and we will not discuss them further. We are, therefore, simulating the inverse Fourier transform to generate the images in the figures using Eq. (3.2) and not using the Fourier series, Eq. (1). We will switch freely between the two forms – sums or

integration – as needed. Eq. (3.2) was used to produce the time-domain function shown along the time axis of Figure 2(B) (the time-domain function is rescaled for the graphics presentation). While this method of calculating the inverse Fourier transform is computationally inefficient, it gives a very clear view of the process.

If we take the approximation for the boxcar, $u(t)$, calculated using Eq. (3.2) and shown in Figure 2(B), and use it to calculate its Fourier transform, we obtain the same set of weights that we started with, as expected and shown in Figure 2(C). As before, to produce the graphic display we are actually calculating

$$c(\omega_n) = \sum_{m=1}^{m_{\max}} u(t_m) \cos(\omega_n t_m + \phi_n) \qquad (3.3)$$

on the computer where t , ω, and ϕ are discretized.

The topographic surface in Figure 2(A) is composed of just the basis function factors of the Fourier transform integrand. The time- and frequency-domain representations are shown on the appropriate axes. To go from one representation to the other, we multiply along one direction and sum along the other as shown by the flow arrows at the top right of Figure 2(A). We can see that the summation and correlation views can be applied to transforming in either direction. The process, but not the FTIV fields (compare Figures 2(B) and 2(C)), is the same. Our natural bias from existing in the real-space domain is what determines which view is the most useful as an explanatory tool for conceptualizing the forward and inverse transforms. One can also see in Figure 2(C) that the boxcar correlates well with the lower frequency components of the basis set, particularly those whose period is greater than the real-space width of the boxcar. The pattern of relative increases and decreases in correlation for the higher frequency components of the basis set contribute to making the corners and sides of the boxcar sharp and vertical.

To better understand how the phase spectrum in the frequency-domain affects the shape of the time-domain function, we will consider a function in which the frequency-domain weights are constant, $c(\omega) = 1$. Since the amplitudes are all equal, the shape of the time-domain function will now be completely determined by the phase spectrum, or how the various sinusoidal components "line up". We will start with the simplest phase spectrum specification in which the phase is a constant independent of frequency and is equal to *0* at $t = 0$, i.e. all the sinusoidal waves "line up" at $t = 0$, shown in Figure 3(A) (which shows the positive frequency portion of Figure 2(A)). This phase spectrum produces a narrow spike in the time-domain located at $t = 0$ which is a delta function, Figure 3(B). In this case of uniform weights and $\phi_n = 0$, it is easy to see the lines of constant phase in the basis function argument of the Fourier transform integrand, as they are also contour lines of constant amplitude in the Fourier transform integrand (Figure 3(A)). This one-to-one relationship between the behavior of the phase argument and the value of the Fourier transform integrand,

$$z\left(t,\omega_n\right)=\cos\left(\omega t+\phi_n\right), \qquad (3.4)$$

for the delta function, that if one is a constant so is the other, holds along any single contour of $z(t,\omega)$. The relationship does not hold between two distinct contours in the Fourier transform integrand having the same value, in which case the phase arguments will differ by $2\pi n$. We will, therefore, equate single contours in the FTIV plot for the delta function with constant value for the phase argument in the remainder of this presentation. This one-to-one relationship between the Fourier transform integrand values and the underlying phase argument is not true in general as can be seen in Figure 2(B) for the boxcar.

We will now use Figure 3 to illustrate a key relationship between the phase argument and the time-domain shape of a function. In Figure 3(C) running sums, or integrations, over frequency are shown along two vertical profiles in the FTIV image. In this case, we know the expression of the function along the vertical integration paths in the Fourier transform integrand, $\cos\left(\omega t\right)$, and note two things: that the integral of this function is non-zero only at $t=0$, where the phase argument is a constant (zero), and that at all other times the integral is zero (small), and the phase argument varies linearly with ω. At $t=0$ all the Fourier transform integrand terms, and their phase arguments, are constant, as indicated by the vertical white ridge through the FTIV image. The running sum at $t=0$ is a linearly increasing function of the frequency. At $t=0.49$, the phase argument varies linearly, and the values along a vertical profile oscillate harmonically, as indicated by the oscillating gray scale along a vertical profile in the FTIV image in Figure 3(C). The running sum or integral over frequency for this oscillating function is also oscillating and remains small. In general the integral of an oscillatory function over a large number of cycles is zero. These two observations are the key to the principle of stationary phase, which says that for functions that are oscillatory over most of their range, the only non-zero contributions to the integral of the function come from the regions where the function is non-oscillatory (e.g. Udías, 1999). We will examine the principle of stationary phase in more detail in the discussion of dispersion. In the following discussion we will refer to the pattern in Figure 3(C) as a skirt pattern, with each line of constant phase argument being a skirt. We will get constructive interference when the skirts are vertical and destructive interference when they are sloping as we cross them along vertical summation or integration paths.

Note that our sum over a finite frequency range, plotted in Figure 3(B), actually produces an approximation to the delta function in the time-domain

$$\int_{-\omega_0}^{\omega_0}\cos\left(\omega t\right)d\omega\propto\frac{\sin\left(\omega_0 t\right)}{\left(\omega_0 t\right)}=\operatorname{sinc}\left(\omega_0 t\right), \qquad (3.5)$$

which is known as the sinc function. If we had taken an exact time-domain boxcar in Figure 2(C) instead of the approximation obtained from Figure 2(B), we would not have

obtained the same sinc function we started with in the frequency-domain (we would still have obtained a sinc function, but of a different width). Eq. (3.5) introduces a fundamental property relating the frequency and real-space extents of a function. The more localized a function is in one domain, the more spread out it is in the other. For ω_0 small, i.e. narrowband in the frequency-domain, $\text{sinc}\left(\omega_0 t\right)$ will be wide in the time-domain, while for ω_0 large, i.e. broadband in the frequency-domain, it will be narrow in the time-domain. The narrowest function in the frequency-domain is a single frequency, a delta function, which is an infinite extent sinusoid in the time-domain. Similarly, as $\omega_0 \to \infty$ in the frequency-domain the width of $\text{sinc}\left(\omega_0 t\right) \to 0$ in the time-domain producing the delta function (Figure 3(B)). Roughly speaking, the product of the widths of the function in the two domains is a constant. This is a general property of the relationship between any Fourier transform pairs. It appears in the wave particle duality concept of quantum mechanics as the Heisenberg Uncertainty Principle, where the probability density functions for both position and momentum, and time and energy, are Fourier transform pairs (Gubbins, 2004). We will see various forms of this integral in the discussions that follow.

Examples

Traveling waves to standing waves and back. To illustrate the features of the FTIV presentation, we will consider two examples. In the first example, we will look at two waves traveling in opposite directions on a string, illustrating the superposition of waves and the relationship between traveling waves and standing waves. In the second example, we will look at a dispersing wave-train and relate the behavior in the frequency-domain to the real-space wave shape and behavior. In order to concentrate on the relationships between the frequency and real-space representations in both cases, we will take the initial disturbance to be a delta function at $x = 0$ and $t = 0$ (Figure 3(A) and (B)).

It is easy to show that functions of the form

$$u\left(x \pm vt\right) \qquad (3.6)$$

in the real-space are traveling wave solutions to the wave equation

$$\frac{\partial^2 u}{\partial x^2} = \frac{1}{v^2}\frac{\partial^2 u}{\partial t^2}. \qquad (3.7)$$

This is known as D'Alembert's solution, and it represents the movement of an arbitrary shaped wave of constant shape at a velocity, v. Consider solutions to the wave equation of the form

$$\cos\left(kx \pm \omega t\right), \qquad (3.8)$$

which represent sinusoidal waves traveling to the left or right, respectively, at velocity

$$v = \frac{\omega}{k} \qquad (3.9)$$

in both the distance-domain and the FTIV space. The argument has been changed to use the wavenumber,

$$k = \frac{2\pi}{\lambda}, \qquad (3.10)$$

in radians/distance unit and the angular frequency,

$$\omega = 2\pi f = 2\pi \frac{v}{\lambda}, \qquad (3.11)$$

in radians/time unit. With this change, the argument is in units of radians, rather than distance, and is related to the wavelength, λ, and angular frequency, ω, of the wave, rather than the velocity. This change ties the argument to the FTIV image, where we can see the wavelength and frequency, but not the velocity. The wave equation is linear, and by the principle of superposition, which allows us to combine solutions to the wave equation to produce new solutions, we can add any number of solutions together to make a new solution. Now consider a solution to the wave equation that is the superposition of two sinusoidal waves that are the same except for their direction of travel

$$u(x,t) = A\cos(kx + \omega t) + A\cos(kx - \omega t). \qquad (4)$$

$$u(k,\omega) = A\cos(kx + \omega t) + A\cos(kx - \omega t). \qquad (4.1)$$

Mathematically either (x,t) or (k,ω) can be the independent variables, which is why we wrote both above, but our bias of living in the (x,t) domain leads us to normally select these as the independent variables. Using simple trig identities Eq. (4) can be rewritten as

$$u = 2A\cos(\omega t)\cos(kx), \qquad (4.2)$$

a sinusoidal wave that is fixed in space, $\cos(kx)$, whose amplitude is modulated harmonically in time, $\cos(\omega t)$. Waves of this type are known as standing or stationary waves. There are a large number of web pages, many of which include animation, that show how the combination of traveling waves produces standing waves, and we do not show that here. The spatial part of Eq. (4.2) is zero, or has "nodes", at $kx = \pi n$ for $n = 1, 2, \ldots$ For a string of length L with both ends fixed, the ends must be on nodes. Letting the ends of the string be at $x = \pm L/2$, we find that for all wavelengths $\lambda = 2L/n$ for $n = 1, 2, \ldots$ both ends of the string are nodes. When pairing the waves as we did here, you see only the standing wave when looking at the sum of the waves. Nothing seems to be going anywhere, as it is in the math of the "matched" traveling waves, but you do not see the traveling waves individually. Note that we have switched the real-space axis from time to distance. The wave in real-space now corresponds to a snapshot,

at a fixed time, of the wavefield in space, similar to a snapshot of the waves on the surface of a pond after having thrown in a pebble. With this change in axis, frequency will mean spatial frequency in cycles/distance unit rather than cycles/time unit, and we will specify frequency using spatial frequency, f_k or wavenumber, k. We could also produce a real-space time series at a fixed position, but the wave snapshot is easier to visualize. The time series gives the time history of the motion at a fixed position, the displacement history of a cork floating in the pond into which we threw our pebble, and the final result is a seismogram. The time and distance-domain figures are indistinguishable in the sense that one cannot tell, without the labeling of the axes, if one is looking at a snapshot of the wave in space or a time history (seismogram) of the wave at a fixed position.

We will now combine the principle of superposition together with Fourier analysis, which says we can make arbitrary functions from weighted sums of sines and cosines. For simplicity, consider the delta function again. Start with two of the delta functions whose FTIV images are shown in Figure 3(A). Let each one propagate at the same velocity, v, with one wave going to the left and the other one to the right (Figures 4(A) and (B)). As all components travel at the same velocity, after a time t_1 the delta functions move without a change of shape to new positions $x = \pm vt_1$. This is just D'Alembert's solution. We can use superposition to add the individual traveling wavefields in Figures 4(A)-ii and (B)-ii directly to obtain the combined traveling wavefield in Figures 4(C)-ii where the waves "pass through" one another. Returning to the two delta functions, since the order in which we do the additions/integrations does not affect the result, we can first combine each pair of Fourier components at a given frequency to make a standing wave at that frequency and then integrate, or sum, these standing waves over frequency. Combining the FTIV fields in Figures 4(A)-i and (B)-i gives the FTIV field shown in Figure 4(C)-i, where one can see patterns reminiscent of, but not the same as, the patterns in the FTIV image for the individual delta functions.

There is another view of the FTIV field shown in Figure 4(C)-i obtained by examining the two parts of the product, $\cos(\omega t)$ and $\cos(kx)$, in the standing wave view, shown on the right side in Figure 4(C)-i. The $\cos(kx)$ part is the same as the delta function in Figures 3(A) and b. At $t = 0$, $\cos(\omega t) = 1$, and the standing wave view has a delta function at $x = 0$. At some later time, $t = t_1$, and remembering that the ω for each Fourier component is a linear function of k (Eq. 3.9, we will reserve writing $\omega(k)$ for the case of dispersive waves where the relationship between ω and k is not linear), the inverse Fourier transform at each position is

$$u(x, t_1) = \int_{-\infty}^{\infty} \cos(\omega t_1)\cos(kx)\,dk = \delta(kx \pm \omega t_1) \qquad (5)$$

by the orthogonality of the cosine functions in the integrand, producing the traveling wave delta functions in Figure 4(C)-ii at positions

$$x = \pm\frac{\omega t_1}{k} = \pm v t_1, \text{ with } -\frac{L}{2} \le x \le \frac{L}{2}. \quad (5.1)$$

At time t_1, therefore, the $\cos(\omega t_1)$ term effectively selects two vertical profiles at $\pm x$ in the FTIV image of the delta function at $x = 0$ that have the same angular frequency as the modulation in time, as is shown graphically in the right hand side of the FTIV image shown in Figure 4(C)-i. The integrand at $\pm x$ is proportional to $\cos^2$, which is $\ge 0, \forall \omega$. At all other locations the integrand is oscillating, and, as we have seen before, integrates to zero.

Another feature of the standing wave viewpoint is that it can generate a more complete construction of the wavefield. The traveling and standing wave views discussed above correspond to two, of several, general approaches to generating synthetic seismograms: ray tracing and modal analysis. Ray tracing has the advantage that each pulse or phase (a new use of the term phase meaning the arrival of a specific pulse, such as the P phase, on the seismogram) in the synthetic seismogram is identifiable and has a known ray path (this corresponds to the process illustrated in Figure 4(C)-ii). The disadvantage is that we only get the phases, or ray paths, we specify. That is one of the reasons we can identify them, and dispersion (which we will do next) cannot be handled easily. In the modal analysis method, we get the complete seismogram, and it is easy to include dispersion, but we cannot easily identify the phases, ray paths, etc. (the process illustrated in Figure 4(C)-i). In the modal view, if we let *t* increase beyond the time for the delta function to travel to the end of the string, it will correctly generate the series of inverted, reflected waves produced each time the waves arrive at the fixed ends of the string. This "feature" can be explained two ways. The first, which works for both the modal and ray tracing views, is based on the infinite extent of the harmonic waves combined with the natural periodicity imposed by the boundary conditions, in our case the fixed ends. In this view the two sets of mathematically defined periodic waves, extending from $-\infty$ to ∞, one going to the right and the other to the left, move into and out of the region $-L/2 \le x \le L/2$ where the string exists. These two waves, as they pass through one another, always combine in such a way that at the ends of the string they cancel to meet the boundary conditions there (fixed). The second is that in the modulated standing wave view, the $\text{mod}(2\pi)$ periodicity of the modulation in time,

$$\cos(\omega t) = \cos(\omega(t + mT)), \quad (5.2)$$

provides the reflected waves, both inside and outside the limits of the string, so it is not necessary to consider infinite extent mathematically defined waves. In a traveling wave or ray tracing view with a D'Alembert type solution, the reflections would have to be done specifically at each end of the string. Both approaches have to take into account the physics and boundary conditions but offer different views of the solution. The modal view for the string is relatively easy to modify for other boundary conditions. For example, a string fixed at one end and free at the other corresponds to taking the traveling

or modal views for the string with both ends fixed and cutting it in the middle, at $x = 0$ (just redraw Figure 4 with the limits at $x = 0$ and $x = \pm L/2$), where the boundary condition for the phase argument of the cosine term at a free end is $\phi = n\pi$, $\forall$n. Reflections from the free end are not inverted, and the maximum amplitude at the free end is double the maximum amplitude of the wave.

We also see in Figures 4(A)-i and (A)-ii that moving, or shifting, the delta function in space (or time) is the same as a phase shift along the space (or time) axis of the $\cos\left(\omega_n t + \phi_n\right)$ terms of the Fourier transform integrand (step 0 in Figure 2). Moving the delta function to $x = x_\delta$, each frequency component in the Fourier transform integrand moves the same "distance" in space (or time), but a different "distance" in phase of the argument, i.e. a different number of wavelengths. This is a graphical view of the Fourier shift theorem

$$F\left(f\left(x - x_\delta\right)\right) = e^{-ikx_\delta} F\left(k\right) = e^{-ikx_\delta} F\left(f\left(x\right)\right). \qquad (5.3)$$

Shifting a wave in space (or time), therefore, does not change its shape or affect the weights of the Fourier components, it only changes the phase spectrum of the components linearly with frequency through the e^{-ikx_δ} term. This is the frequency-domain expression of translational invariance in the time- and distance-domains. There is also a breakdown in the symmetry between the forward and inverse Fourier transforms here as the phase shift for both the forward and inverse Fourier Transform is always parallel to the real axis (step 0 in Figure 2). There is no equivalent to translational invariance in the frequency-domain, where the origin is unique.

Dispersion: Next consider the case of a traveling wave in a medium in which the velocity of wave propagation is a function of frequency, i.e. a wave traveling in a dispersive medium. If each frequency component propagates at its own velocity, $v\left(f_k\right)$ (or $v\left(k\right)$), two things happen as the wave propagates for some time t. First, as before, the position of the wave moves to a new location. Second, and more interestingly, is that the shape of the wave changes. This does not correspond to a D'Alembert type solution. The FTIV image can be used to illustrate several aspects of the evolution of the wave shape as a function of time, and the development of this method, applied to seismic surface wave analysis, was first presented in Brune, et al. (1960) and Nafe and Brune (1960). We will now examine this case, focusing on the relationship between the Fourier transform space and real-space shapes, illustrated in Figure 5, in more detail. Detailed mathematical presentations and insights into the physics can be found in Brune et al. (1960) and Nafe and Brune (1960) and in most intermediate and advanced seismology textbooks (Båth, 1968; Achenback, 1973; Udías, 1999; Aki and Richards; 2002; Pujol, 2003).

Starting as a delta function shown in Figures 3(A) and (B), after some time t_1, the individual harmonic waves will each travel at their own velocity some distance,

$$x = v(k)t_1, \qquad (5.4)$$

producing the FTIV image and real-space plots, shown in Figures 5(A) and (B). The frequency and real-space domains are now related by

$$u(x,t) = \int_{-\infty}^{\infty} \cos\left(kx - \omega(k)t\right) dk \qquad (5.5)$$

(Brune et al., 1960, Nafe and Brune, 1960) where

$$\omega(k) = kv(k). \qquad (5.6)$$

The vertical line of constant phase (of the argument) originally at $x = 0$ and $t_0 = 0$ in Figure 3(A) gets sheared into a new shape at t_1 shown by the cyan line in Figure 5(A) (step 0 in Figure 2). By rescaling the x axis in Figure 5(A) by $1/t_1$, the axis can be changed to units of velocity, and we can use the same figure to plot velocity as a function of frequency and a velocity axis is drawn across the top of Figure 5(A). The cyan line is, therefore, also a plot the of the velocity at which the waves in the FTIV field move as a function of frequency, $v(k)$. The velocity distribution used here was constructed to be differentiable and produce dispersion similar to that for surface waves in the earth, where the longer wavelength, lower frequency waves propagate faster. In this example, the velocity distribution has constant velocity segments for the lowest and highest frequencies, traveling at speeds v_1 and v_2, respectively, and varies smoothly and monotonically between them. As time increases, part of the vertical skirt at $x = 0$ and $t_0 = 0$ becomes sloping, and we find a new collection of points, (x,k), in the FTIV image shown by the magenta line where the initially sloping skirts deform such that they now have a fold at which point they go through vertical.

We will now examine the development of the real-space wavefield in Figure 5(B) from the initial shape. Compared to the delta function, the traveling wavefield has some wider, more complicated shape that is confined approximately to the region $v_3 t_1 < x < v_1 t_1$. Note that the x axis in Figures 5(A) and (B) is shifted, or panned, to follow the center of the dispersing wave-train. The observed width of the wavefield is wider than what one would expect if the width was based on the fast and slow limits of the velocity distribution, $v_2 t_1 < x < v_1 t_1$. From where does this low velocity limit, v_3, which is not a physical velocity of the medium, arise? The answer can be illustrated through analysis of the skirt pattern.

To assist in the discussion of the details of the dispersed wave-train, we will divide both axes of the plot of the (x,k) space into a number of regions. The divisions along the frequency axis are indicated by the horizontal lines α through δ in Figure 5(A) and divide the magenta curve, which we will discuss shortly, into five branches labeled I through V. Using the lines v_1, v_2, and v_3 of the velocity axis of Figure 5(A) for reference, the real-space axis can also be divided into the region to the left of v_1, where

the skirts all slope to the left, a narrow region about v_1; the region between the lines for v_1 and v_2, where the skirts are folded over a single time; a narrow region about v_2, a region between v_2 and v_3, where the skirts are folded over twice with the folds facing opposite directions; a narrow region about v_3, where the slope of the skirts goes through vertical without a fold; and finally a region to the right of v_3 where the skirts all slope to the right. We will call the regions V1L, V11, V12, V22, V23, V33, and V3R respectively.

Returning to the FTIV image of the dispersed wave in Figure 5(A), we observe that in regions V1L and V3R the skirts, or lines of constant phase (of the argument), are all sloping outward, similar to the skirts in Figure 3(A), and integration along vertical paths there will be zero. An example of this is shown by the oscillatory integrand and small running sum (integration) in Figure 5(C)-i. The wavefield at time t_1 will, therefore, not be found in regions V1L or V3R, outside the approximate limits V11 and V33.

We will next look at the region V11, where the skirt pattern is vertical for $0 < k < \alpha$, where all the Fourier components arrive traveling at a constant velocity, v_1, and then slopes for $\alpha < k$. Remembering that regions of the integrand where the skirts slope do not contribute to the integral, we can limit our integrand to the range $0 < k < \alpha$. We might expect these waves to combine into a wave of some shape that also travels at v_1 and we will see that this is the case. Consider the integration over a finite range of continuous frequencies, all traveling at the same velocity, v_1,

$$u(x,t) = \int_{k_0-\delta k}^{k_0+\delta k} \cos(kx - \omega t)\, dk\,, \qquad (5.7)$$

where $u(x,t)$ is the wavefield in the distance-domain. This integral looks very similar to Eq. (3.5) and evaluating it (Udías, 1999) gives

$$u(x,t) \propto \frac{\sin(X)}{X}\cos(k_0 x - \omega_0 t) = \mathrm{sinc}(X)\cos(k_0 x - \omega_0 t)\,, \quad X \propto (x - v_1 t)\delta k\,, \quad (5.8)$$

which is the product of a carrier, $\cos(k_0 x - \omega_0 t)$, where $\omega_0 = k_0 v_1$, with a sinc modulation function. (We are again concentrating on the principal properties of the solution and are continuing to ignore the scaling – see the texts referred to earlier for full solutions). The carrier is simply a traveling sinusoid with wavenumber k_0, and frequency ω_0. In the argument of the sinc function, the $(x - v_1 t)$ term shifts the location of the sinc function by $v_1 t$, while the δk term controls the width. The relationship between δk and k_0 determines the shape of $u(x,t)$. For k_0 small (long wavelength) and δk "large" the sinc function is narrower than the wavelength of the traveling sinusoidal wave, and the resulting shape looks like a sinc pulse, as can be seen in the leading wiggle of the wavefield near $x \approx -7.5$ and labeled ii, in Figure 5(B). For k_0 large (short wavelength) and δk "small" the sinc function is wider than the wavelength of the traveling sinusoidal wave and the resulting wave shape looks like a sinc modulated sinusoidal wave group or packet. This can be seen in region V22 where the skirt pattern is also vertical in the high frequency range, $\delta < k < k_{\max}$, and all the Fourier components travel at a

constant velocity, v_2. Here we find a sinc modulated wave packet of high frequency sinusoidal waves at location iv, near $x \approx 3.5$, in Figure 5(B). In regions V11 and V22 the sinc modulation envelopes move at the same velocity as the component waves (parts I and V of the velocity plot). In Figures 5(C)-ii and (C)-iv the integrand and the running sums (integrations) are plotted, and we can see that the contributions to the real-space wavefield come from the regions in gray, where the velocity, integrand and integrand phase are all constant. In both V11 and V22, the sinc modulation restricts the resulting real-space wavefield to a pulse or wave packet over a finite region of space moving at v_1 or v_2 respectively, and we can see that this region contains the energy or information carried by the wave. In this case, the real-space wave packet or pulse travels at the same velocity as the component waves in the FTIV image (cyan curve). We will see shortly, that this is not always the case, and we will need to distinguish between two velocities.

We will now look at regions V12 and V23 where the skirts have one or two individual folds. In this region, we find that the wiggles in the wavefield do not travel at the velocity shown by the cyan curve but travel at a velocity defined by sections II-IV of the magenta curve in Figure 5(A). We will now introduce the term group velocity for the velocity at which waves travel in the real-space with their energy and information (magenta curve) and the term phase velocity for the velocity of the individual component waves and the velocity at which they travel in the FTIV field (cyan curve). Note that a single frequency wave would travel at the phase velocity. We will now investigate these velocities, especially the group velocity, more thoroughly.

Before discussing Figure 5 in more detail, we will first examine the basic ideas of phase and group velocity by looking at the simplest case in which the two velocities are different; the superposition of two sinusoidal waves at slightly different frequencies or wavelengths, traveling at slightly different phase velocities. For a smoothly varying velocity, start with a reference wave traveling at some wavenumber k and velocity $v(k)$ and construct two new waves at wavenumbers

$$(k \pm \delta k), \qquad (5.9)$$

traveling at velocities

$$v(k \pm \delta k) = v(k) \pm \frac{dv(k)}{dk}\delta k, \qquad (5.10)$$

with frequencies

$$\omega \pm \delta\omega = v(k \pm \delta k)(k \pm \delta k), \qquad (5.11)$$

under the condition that

$$\delta k << k, \delta\omega << \omega. \qquad (5.12)$$

Combining these two waves we obtain

$$F = A\cos\left(\left(k+\delta k\right)x-\left(\omega+\delta\omega\right)t\right)+A\cos\left(\left(k-\delta k\right)x-\left(\omega-\delta\omega\right)t\right), \qquad (5.13)$$

which, as before, can be rewritten as

$$F = 2A\cos\left(kx-\omega t\right)\cos\left(\delta k\,x-\delta\omega t\right). \qquad (5.14)$$

This could be broken down further into functions of $\left(kx\right)$, $\left(\omega t\right)$, $\left(\delta k\,x\right)$ and $\left(\delta\omega t\right)$ but doing so does not provide additional physical insight. In the real-space domain this is the product of two traveling waves, one traveling at a velocity

$$v\left(k\right)=\frac{\omega\left(k\right)}{k}, \qquad (5.15)$$

and the other traveling at a velocity,

$$\frac{\delta\omega\left(k\right)}{\delta k}=v\left(k\right)+k\frac{dv\left(k\right)}{dk}=U\left(k\right). \qquad (5.16)$$

We recognize the first velocity, Eq. (5.15), as the phase velocity of the reference wave. The second velocity is new and does not correspond to the velocities of the waves used in the superposition, but to the velocity of the second traveling wave factor in Eq. (5.14), and this velocity is called the group velocity. If all the waves travel at the same phase velocity, $dv\left(k\right)/dk=0$, and $U\left(k\right)=v\left(k\right)$, there is no need to distinguish between phase and group velocities, or carry around the k dependence, although using the term group velocity ensures we are talking about the velocity of energy propagation.

The standard presentation of the relationship between the phase and group velocity is shown in Figure 6(A), while a 3D surface view is shown in Figure 6(B). In this simple case, one can determine the phase velocity by measuring the wave at two or more positions and finding the velocity at which the wiggles travel (the slanted dashed red line in Figure 6(A) follows the crest of a wiggle). One has to be careful to not "skip" wiggles, by an integer number of wavelengths, which can easily happen if the measurement points are too far apart as the wiggles are indistinguishable. The group velocity, shown by the slanting green line in Figure 6(A), is determined by measuring the wave envelope at two or more positions to find the velocity of the envelope. This may be difficult as the envelope is not well defined when there are a small number of wiggles in the envelope. Determining group velocity also suffers from the wiggle skipping problem, as the groups are also indistinguishable, but with respect to the envelope which skips in steps of half its wavelength. If one sits on the "envelope" of a group of waves, one travels at the group velocity and the wave crests run by underneath at the phase velocity (the waves in the group can run forward, backward or, if $v=U$, be stationary).

As we saw above, energy is carried by the wave at the group velocity as this is the

velocity at which the waves arrive, or are observed, in the real-space. This is not obvious with the infinite extent waves in Figure 6, but one can get an idea of how this works if one surfs a crest of the waveform (the one on the left marked in red in Figure 6(B) for example). One moves at the phase velocity, but the wave "runs out" in the trough and you get dumped in the water and have to wait for another crest from behind to surf forward again (the crest on the right in Figure 6(B) marked in red for example). This new crest also runs out when it arrives at the trough, and you have to catch a later crest again. You are basically limited to catching the crests in one modulation package of the envelope. Your long term average forward speed, therefore, is the speed at which the envelope travels, which is the group velocity. This analogy does not work when the phase velocity is less than the group velocity. In this case, energy still travels at the group velocity, which can be seen if the surfboard is long enough that it is surfing the envelope, rather than the individual wave crests, and again moves forward at the group velocity. As in the case of the traveling-standing wave combination, there are many animations on the web of this effect.

We can now apply these ideas to the dispersing wave-train in Figure 5, which illustrates graphically the observation that phase velocity is an easy concept to understand, but a hard quantity to measure as nothing is physically traveling at the phase velocity, and that group velocity is a hard concept to understand, but an easy quantity to measure, as this is the velocity at which the physical wavefield travels. If one jumps on a crest of the real-space wave, one finds the crest to have some wavelength and be traveling at some velocity. As one rides along with that crest, however, both the wavelength and the velocity change with time. Both changes are directly related to the evolution of the fold in the skirt pattern in FTIV space with time. We will see that at any time, riding on the crest of the wave at x, with wavenumber k, in real-space is equivalent to riding at the same position, x, on the crest of the Fourier component that has the same frequency in FTIV space. As time progresses, however, the skirt changes shape and moves through FTIV space sampling other frequencies and phase velocities. If one wants to follow an individual crest in the real-space domain, one has to change frequencies and, therefore, velocities, in FTIV space by following the magenta group velocity curve in Figure 5(A). The distinction between the phase and group velocities is clear in the FTIV space as is the relationship of the evolution of the skirt pattern in FTIV space to the velocity and shape of the waves in the real-space.

To illuminate the relationship between the patterns seen in the FTIV space and the shape of the real-space function we will now return to the discussion of the principle of stationary phase. In its general form, the principle of stationary phase, first outlined by Cauchy (Erdelyi, 1955) and fully developed by Stokes and Kelvin (Båth, 1968), considers integrands which are the product of two functions, a slowly varying function, $\varphi\ (k)$, and an oscillatory function, $e^{i\Psi(k,x)}$,

$$f(x) = \int_a^b \varphi(k) e^{i\Psi(k,x)} dk \qquad (5.17)$$

(Båth, 1968). In addition to providing insight into the propagation of dispersed waves, the principle of stationary phase provided an important trick that facilitated evaluation of the inverse Fourier transform when "computers" were people. These two points were actually the motivation for its development, although it can also be derived by modern analysis techniques. By using the delta function in the real-space domain, we only have to consider the oscillatory term, $e^{i\Psi(k,x)}$, since $\varphi(k) = F(\delta) = 1$. This greatly simplifies the discussion of stationary phase without losing the insight.

We will now apply our earlier observation in Figure 3(C), that the only non-zero contributions to the inverse Fourier integration come from regions where the phase of the argument of the integrand is a constant, or equivalently its derivative is zero. We have to remember that while individual contour lines of the image in Figure 5(A) have constant values of the function

$$F(k,x) = \cos\left(kx - \omega(k)t\right) \qquad (5.18)$$

they are not contours of the argument

$$\left(kx - \omega(k)t\right) \qquad (5.19)$$

directly, but they can be interpreted as lines of constant phase of the argument when the Fourier weights are constant. On any single contour line we will consider

$$f(k,x) = \text{constant , or } \left.\frac{\partial f(k,x)}{dk}\right|_x = 0 \qquad (5.20)$$

to be equivalent to

$$\Psi(k,x) = \left(kx - \omega(k)t\right) = \text{constant , or } \left.\frac{\partial \Psi(k,x)}{\partial k}\right|_x = 0 \text{ , and } \frac{x}{t} = \left.\frac{d\omega(k)}{dk}\right|_x = U(k), \qquad (6)$$

which says the contribution to the wavefield from the Fourier component k arrives at x at the group velocity, $U(k)$.

In region V12, after the large initial arrival, we find an extended train of sinusoidal waves whose wavelength (this is a wavefield snapshot) slowly decreases. Looking at the integrand and running sum in Figure 5(C)-iii we can see that the major contribution to the wavefield in region V12 comes from the small region, indicated by the gray background, which comes from the area around the fold in the skirt pattern in the FTIV image in Figure 5(A), where the slope is vertical or the phase of the argument in the inverse Fourier transform integrand is stationary. A frequency, k, that has a stationary phase, i.e. a vertical skirt in Figure 5(A), defines a single point (x_0, k_0) in the FTIV space. The magenta line in Figure 5(A) connects the points (x,k) in the FTIV that have stationary phase and defines the group velocity, the velocity at which the observed

waves of each wavelength, and the energy associated with them, travels. In region V12, one branch of stationary phase is found at long wavelengths and produces a wavefield of sinusoidal wiggles at a slowly varying instantaneous frequency. In region V23, we find two branches of stationary phase: one along a continuation of the magenta curve from region V12, and a separate one at shorter wavelengths. By superposition, we add the results from each branch of stationary phase individually as shown in Figure 5(C)-v, where we again see that the non-zero contributions to the final value at that position comes from the two branches of stationary phase, shown in gray. If we divide the frequency axis between α and δ into two parts about the frequency where the group velocity turns around ($f_k \approx 110$) and integrate each part individually, the real-space dispersed wave-train from the low frequency part has increasingly shorter wavelengths as one goes from v_1 to v_3. This effect is clearly seen in region V12, and is called normal dispersion. The sum for the higher frequency part has increasingly shorter wavelengths as one goes from v_3 back to v_2 and this is called anomalous dispersion. In region V23, the two patterns are superimposed, making them hard to see individually. We also note here that in order to use the principle of stationary phase, which is an approximation, we have to let the wave propagate for sufficient time such that the integrand is highly oscillatory over all its range (skirts are sufficiently sheared) except for the immediate region of the stationary phase. This is typically true for travel times that are much greater than the periods of the frequency components about the point of stationary phase (Pujol, 2003).

Performing the inverse Fourier transform in regions V12 and V23 requires evaluating Eq. (5.5). This integral cannot, in general, be evaluated in closed form due to the $\omega(k)$ term. While the details of the mathematics in this next section can get quite complicated, the basic method is straightforward. We have seen that only a small region of the range of integration about the point of stationary phase contributes to the value of the integration. We will, therefore, concentrate on evaluating the integral in that region and the final result will turn out to be relatively simple. For well behaved integrands, the integral in the region of interest can be approximated using a Taylor series expansion of the argument to the integrand about a point of stationary phase, (k_0, x_0), to find $u(x_0, t)$. From Eq. (6) we saw that the contribution to the wavefield from the Fourier component k_0 arrives at x_0 at the group velocity, $U(k_0)$. Keeping the lowest non-zero term of the Taylor series expansion of $\Psi(k, x)$ about the point of stationary phase, where $\omega' = 0$, and using the prime to represent d/dk

$$\Psi(k_0, x_0) \approx k_0 x_0 - \left(\omega_0 + (1/2)(k - k_0)^2 \omega''(k_0)\right) t \qquad (6.1)$$

Plugging this into Eq. (5.5), using the exponential form Eq. (5.17) to make the integration easier (we will take the real part at the end), using Eq. (6), noting that the integral outside the neighborhood of k_0 is null so the limits can be expanded to $\pm\infty$, doing a little algebra, and again ignoring scaling constants our approximation becomes

$$u(x_0,t) \propto \mathrm{e}^{i(k_0 x_0 - \omega_0 t)} \int_{-\infty}^{\infty} \mathrm{e}^{i\left(-(t/2)U'(k_0)(k-k_0)^2\right)}\, dk\,, \qquad (6.2)$$

which shows that $u(x_0,t)$ will be a traveling sinusoidal wave, represented by the

$$\mathrm{e}^{i(k_0 x_0 - \omega_0 t)} \qquad (6.3)$$

term, multiplied by whatever the integral comes out to be. To evaluate the integral, substitute

$$\Omega^2 = (t/2)U'(k_0)(k-k_0)^2\,, \;\; \Omega\, d\Omega = (t/2)U'(k_0)(k-k_0)\, dk\,, \qquad (6.4)$$

to obtain

$$u(x_0,t) \propto e^{i\left(k_0 x_0 - \omega_0 t\right)} \left(U'(k_0)\right)^{-1/2} \int_{-\infty}^{\infty} e^{-i\Omega^2}\, d\Omega\,, \qquad (6.5)$$

which is a form of the Fresnel integral. This can be evaluated using contour integration (Båth, 1968)

$$\int_{-\infty}^{\infty} e^{-i\Omega^2}\, d\Omega \propto e^{\left(i(\pi/4)\operatorname{sgn} U'(k_0)\right)}\,, \qquad (6.6)$$

to provide a simple result - a complex valued constant that changes the amplitude, which we are ignoring, and the phase, upon which we are concentrating, of $u(x_0,t)$. Plugging this into Eq. (6.2) and taking the real part

$$u(x_0,t) \propto \left(U'(k_0)\right)^{-1/2} \cos\left(k_0 x_0 - \omega_0 t + \pi/4 \operatorname{sgn} U'(k_0)\right), \qquad (6.7)$$

we find the wavefield to be a sinusoidal traveling wave of instantaneous frequency, f_{k_0}, moving at the phase velocity,

$$v = \frac{\omega_0}{k_0}, \qquad (6.8)$$

that arrives at x_0 at the group velocity,

$$U = \frac{\delta\omega}{\delta k} = \frac{x_0}{t_a}, \qquad (6.9)$$

where t_a is the arrival time. The instantaneous frequency at x_0 is the same as the frequency at which the phase of the argument is stationary, but the wavefield has a $\pm\pi/4$ phase shift with respect to the sinusoidal Fourier transform integrand component. This phase shift, which is a subtle effect, can be seen by comparing the position where the bright part of the skirt in the Fourier transform integral is vertical with the position of the crest of the dispersed wavetrain (difference shown by the short sideways "T" on the

reference line iii in Figures 5(A) and (B)). The sign of the phase shift is determined by the sign of the second derivative, or graphically, the direction the fold in the FTIV space is facing. We have kept the subscript on x because the k_0, where the phase of the argument is stationary, determines x_0 (and ω_0). We have also kept one amplitude scaling term, as it will contribute to the following discussion. When we evaluated the integrals in Eq. (3.5) and Eq. (5.7), it was not essential to examine the phase of the argument of the Fourier transform integrand. Doing so, however, prepared the background for evaluating Eq. (5.5), where the effect of the spectral phase shift in the frequency-domain on the phase argument of the Fourier transform integrand is what determines the wavefield shape and velocity in the distance-domain.

This leaves region V33, which is an inflection point where the second derivative of the phase of the argument is also zero, as indicated by the skirts going vertical but not forming a closed fold. Even though the argument phase is stationary here, we cannot use the method of stationary phase as presented above to estimate $u(x,t)$ because the term $\omega''(k_0) = U'(k_0)$ in the denominator in Eq. (6.7) is now zero. We will find that there will be a larger constructive interference effect here as the group velocity is now also constant. Here again, while the details are complicated, the procedure is straightforward, and the result will be simple. The usual solution to estimate the waveform here is to carry the Taylor series approximation of Eq. (6.1) one derivative further to

$$\omega'''(k_0) = U''(k_0) \neq 0 . \qquad (6.10)$$

Temporarily relaxing the stationary phase requirement that $\omega'(k_0) = 0$ allowing us to keep the first derivative term, and keeping the third derivative term, following Savage (1969), we have

$$\Psi(k_0, x_0) \approx k_0 x_0 - \omega_0 t + (k - k_0)\left(x_0 - \omega'(k_0)t\right) + \tfrac{1}{6}(k - k_0)^3 \omega'''(k_0)t \qquad (6.11)$$

and

$$u(x_0,t) \propto e^{i(k_0 x_0 - \omega_0 t)} \int_{-\infty}^{\infty} e^{\left((k-k_0)(x_0 - \omega'(k_0)t) + \frac{1}{6}(k-k_0)^3 \omega'''(k_0)t\right)} dk , \qquad (6.12)$$

a traveling wave multiplied by the result of the integral, similar to Eq. (6.2). To evaluate the integral make the substitutions

$$\Omega = \left(\tfrac{1}{2}\omega'''(k_0)t\right)^{\frac{1}{3}}(k - k_0), \text{ and } \frac{d\Omega}{\left(\tfrac{1}{2}\omega'''(k_0)t\right)^{\frac{1}{3}}} = dk \qquad (6.13)$$

and remembering $\omega' = U$ we obtain

$$u(x_0,t) \propto e^{i(k_0 x_0 - \omega_0 t)} U''(k_0)^{-\frac{1}{3}} \int_{-\infty}^{\infty} e^{i\left(b\Omega - \frac{1}{3}\Omega^3\right)} d\Omega \qquad (6.14)$$

$$\text{with} \quad b = \left(x_0 - \omega'\left(k_0\right)t\right)\left(\tfrac{1}{2}\omega'''\left(k_0\right)t\right). \qquad (6.15)$$

The integral in Eq. (6.14) is known as the Airy integral (Airy, 1838), and it produces the Airy function, Ai, which can also be used to model Rayleigh wave dispersion (Savage, 1969). When not at an inflection point the solution is of the form

$$u\left(x_0,t\right) \propto e^{i\left(k_0 x_0 - \omega_0 t\right)} U''\left(k_0\right)^{-1/3} Ai\left(\text{argument} \propto \left(x_0 - \omega'\left(k_0\right)t\right)\right). \qquad (6.16)$$

As we found before, this is a traveling wave of instantaneous frequency, f_{k_0}, moving at the phase velocity, $v = \omega_0 / k_0$, that arrives at x_0 at the group velocity, $U = \delta\omega/\delta k = x_0/t_a$, where t_a is the arrival time, modulated by the Airy function. At an inflection point, which is our case, we reapply the condition for stationary phase. This gives $b = 0$ in Eq. (6.15), and the value of the Airy function reduces to a number (not a traveling wave term) and

$$u\left(x_0,t\right) = e^{i\left(k_0 x_0 - \omega_0 t\right)} U''\left(k_0\right)^{-1/3}, \qquad (6.17)$$

which again is a traveling wave of instantaneous frequency, f_{k_0}, moving at the phase velocity, $v = \omega_0 / k_0$, that arrives at x_0 at the group velocity, $U = \delta\omega/\delta k = x_0/t_a$, where t_a is the arrival time. In this case, the wavefield is in phase with the corresponding component in the FTIV space, as one might expect as the folding of the skirts is not closed and the region that interferes constructively is more symmetric. As in Eq. (6.7) we have kept one scaling term, and comparing it and Eq. (6.17), we see that the latter decreases more slowly than the former. The stronger constructive interference, due to both the phase and group velocities being constant, produces a slower decrease in amplitude to make the wavefield at the x value associated with the inflection point relatively large, as can be seen in Figure 5(B). This large pulse in the wavefield is called the Airy phase, and it is associated with an extremum, in this case the minimum, of the group velocity at which point the wavefield effectively turns off.

Figure 7 shows the time evolution of the wavefield, which turns out to be relatively simple when viewed this way. The origin of the x axis tracks the center of the wavefield, so it represents a point that is moving through space at a "reducing velocity" of

$$v_r = \frac{v_1 + v_3}{2}. \qquad (6.18)$$

We observe two sinc modulated groups (pulses) traveling at v_1 and v_2 respectively and the Airy phase pulse at the back traveling at v_3 at which point the wavefield shuts down. Parts a, b, and c in Figure 7 each look along a line following one of the three fundamental velocities (v_1, v_2 and v_3, respectively) of the dispersion relationship. New wiggles in the wavefield arise out of the Airy phase traveling at v_3 at the back (right) side and travel

within the dispersed wave-train at a changing group velocity and instantaneous frequency to the left, sub-parallel to their limiting velocities, v_1 for the low frequency component, and v_2 for the high frequency component. Each wiggle is permanent; the wiggles do not coalesce once they arise. The wiggles from the lower and higher freq branches in V23 can be seen individually in the views a, b, where they are subparallel to v_2, and c where the interfering wiggles modulate the wavefield.

The dispersion curve was constructed to illustrate several different aspects of dispersed wavefield development in the earth, but is not a realistic earth dispersion curve. The low frequency branch V12 and V23 has a large change in group velocity over a small frequency range, producing a long train of sinusoidal wiggles in the wavefield similar to the case of oceanic Rayleigh wave dispersion. As time goes on in Figure 7(A), the folds along V12, V23 and V32 get tighter and narrower and move to lower frequency. Additionally, as the distance between the leading and trailing edges of the wavefield, traveling at v_1 and v_3 gets larger (longer) more "wiggles" have to fill this region. New wiggles arise as additional folds are created on the low and high frequency limits, β and γ, at V33, and each wiggle is composed of a narrow range of component waves and delayed by a cycle, 2π in argument phase, with respect to the wiggle in front of it. The flat "bucket" in the group velocity at v_3, between β and γ, makes a strong Airy phase beyond which the wavefield quickly shuts off, similar to the Airy phase of continental Rayleigh waves. We can clearly see that while motion of the waves in the FTIV field move at the phase velocity, this velocity has little or no physical significance in the real-space (distance-domain). Similarly, while we do not see the component waves moving at the group velocity in the FTIV field, we do see structure there. This structure, associated with the velocity of the modulating envelopes or the instantaneous frequency, produces the group velocity, which is the velocity energy and/or mass is transported in the real-space domain.

In the case of analyzing dispersed surface waves from a real earthquake, we have to consider the actual source, which will not in general be a delta function. For the analysis of teleseismic surface waves, the main consideration will be the specification of an initial phase spectrum at the source as the amplitude spectrum is uniform (Brune, 1970). In addition, when calculating synthetic seismograms for comparison to seismograms recorded at teleseismic distances, since phase measured from the seismograms can only be determined to $\mathrm{mod}(2\pi)$, one has to find the total distance by including the number of whole cycles between the source and receiver that are lost due to the $\mathrm{mod}(2\pi)$ (Brune et al., 1960). This is the same as the "integer ambiguity" problem when using GPS phase measurements to determine position.

So far we have considered surface waves from only the traveling wave standpoint. As we saw earlier, by combining the wavefields of dispersing surface waves traveling in opposite directions, we obtain a modal or standing wave view. As the wavelengths of surface waves approach the size of the earth, and the waves have to "fit" around the earth this becomes the natural view. We will not present an image of this combination, but the

results in the FTIV space will be similar to those for the two delta functions in Figure 4, and the two dispersing wavetrains will not affect one another in the real-space domain. While it is easy to visualize changing the linear string to a circle, the modal view on a sphere requires changing the basis functions to spherical harmonics.

Discussion

We have seen that the phase spectrum, i.e. how the phase shifts in the frequency-domain vary as a function of frequency, can have a large effect on the real-space, time or distance-domain, shape of the function. How does this compare to the effects of changing the amplitude spectrum, or how the weights vary as a function of frequency? In general it is difficult to visually interpret plots of time-domain signals and the effect filtering (which in general changes both amplitude and phase) has on them in terms of the information, etc. the signal carries. It is instructive, and easy to do using tools such as Matlab® for example, to record and play back a voice recording to investigate the effects of varying either the amplitude or phase spectra on the playback. If the amplitude spectrum is randomized or made uniform, the playback is easily recognizable and understandable, but noisy. If the phase spectrum is randomized, however, the playback is a white noise and completely unintelligible. If the phase spectrum of a voice recording is modified smoothly and nonlinearly, a linear variation just moves the playback in time as per the shift theorem, the length of the playback will usually change with respect to the length of the recording. This change in length is not due to just a slowing down or speeding up of the playback, as would happen if one varied the speed of a tape recorder on playback. The change in length is due to the nonlinear phase shift, the same as was the case in the dispersing wave discussed earlier. For small amounts of dispersion, this causes interesting effects in the playback, but for sufficient dispersion, the playback becomes unintelligible.

Previously we saw that the delta function was composed of all frequencies with the same weight with their phases equal to zero at the location of the delta function and that we could generate a dispersed seismogram from the delta function by a specific variation of the phase spectrum. The same amplitude spectrum, all weights equal, but with the phases randomized results in white noise. Similarly, amplitude spectra with weights proportional to f^{-2}, f^{-1}, f^{1} and f^{2} with random phase spectra produce red or brown noise, pink noise, blue and violet noise, respectively. Using these spectra rather than uniform weights, with $\phi(\omega) = 0$ at $t = 0$, as the initial frequency-domain specification would have produced similar dispersed seismograms as the dispersion example illustrated, but with either the high or low frequencies accentuated. For the case of the boxcar, which has $\phi(\omega) = 0$, it is the amplitude spectrum that defines the basic shape. If the boxcar travels in a dispersive medium, it initially disperses into a wider, complicated shape whose evolution cannot be described easily. For travel times much, much greater than the width of the boxcar, the dispersed boxcar looks similar to a modulated version of the dispersed delta.

The delta function, white noise, and the dispersed wavetrains discussed above all have the same amplitude spectrum, but very different real-space functions, and the real-space functions in this case are determined by the phase spectrum. When processing seismograms, it is important to clearly understand where, i.e. in which domain – time or frequency – the information lies. If one is studying surface waves, the information is in the phase, which is in the frequency-domain. In this case, one has to be careful to insure the observed phases are caused by the earthquake and transmission through the earth and not the processing. Conversely, if one is measuring arrival times of body wave phases, the information is in the time-domain. One now has to insure that the processing does not change when the phases arrive (start). In this case, any frequency-domain processing has to modify the frequency-domain phase such that it does not cause the seismic phase arrival in the time-domain to become acuasal (which is what happens in the simple case of the band limited delta function in Eq. 3.5; the center of the sinc function is at the same time as the original delta function, but the wiggles "start" earlier and continue later). Frequency dependent attenuation, which is a filter, therefore, requires dispersion to maintain causality.

Conclusion

We have seen that viewing the Fourier transform integrand as a topographic surface can provide insight into a number of features of wavefields in the real-space domain. For many types of observation, the phase spectrum carries the information about both the source of the waves and the path over which they travel. Understanding the effect of the phase spectrum on the real-space function can be key to recovering this information. The FTIV presentation provides insight into the often underappreciated contribution of the phase spectrum to the shape of the real-space function, of how to make traveling waves from standing waves, of the traveling wave versus modal models of generating waves, and the behavior of dispersing wavefields. It also illustrates the symmetry between the forward and inverse Fourier transform.

Acknowledgements

I thank C. Langston, J. Pujol, M. Bevis, and SRL editor L. Astiz for helpful reviews.

References

Airy, G. B. On the intensity of light in the neighborhood of a caustic. Trans. Cambridge Phil. Soc., 6:379–403, 1838.

Achenback, J.D., Wave Propagation in Elastic Solids, North Holland, NY, 424pp, 1973.

Båth, M., Mathematical Aspects of Seismology, Developments in Solid Earth Geophysics, 4, Elsevier, NY, 415 pp, 1968.

Brune, J.N., J.E. Nafe, and J.E. Oliver, A Simplified Method for the Analysis and Synthesis of Dispersed Wave Trains, J. Geophys. Res., 65, 1, 287-304, 1960.

Brune, J., Tectonic Stress and the Spectra of Seismic Shear Waves from Earthquakes, J. Geophys. Res., 75(26), 4997-5009, 1970.

Erdelyi, A., Asymptotic Representations of Fourier Integrals and the Method of Stationary Phase, J. Soc. Indust. Appl. Math., 3, 1, 17-27, 1955.

Gubbins, D., Time Series Analysis and Inverse Theory for Geophysicists, Cambridge University Press, Cambridge, 255 pp, 2004.

Nafe, J.E., J.N. Brune, Observations of phase velocity for Rayleigh waves in the period range 100 to 400 seconds, Bull. Seis. Soc. Am., 50, 3, 427-439, 1960.

Pujol, J., Elastic Wave Propagation and Generation in Seismology, Cambridge University Press, Cambridge, 444 pp, 2003.

Savage, J.C., A New Method of Analyzing the Dispersion of Oceanic Rayleigh Waves, J. Geophys. Res., 74, 10, 2608-2617, 1969.

Udías, A., Principles of Seismology, Cambridge University Press, Cambridge, 475 pp, 1999.

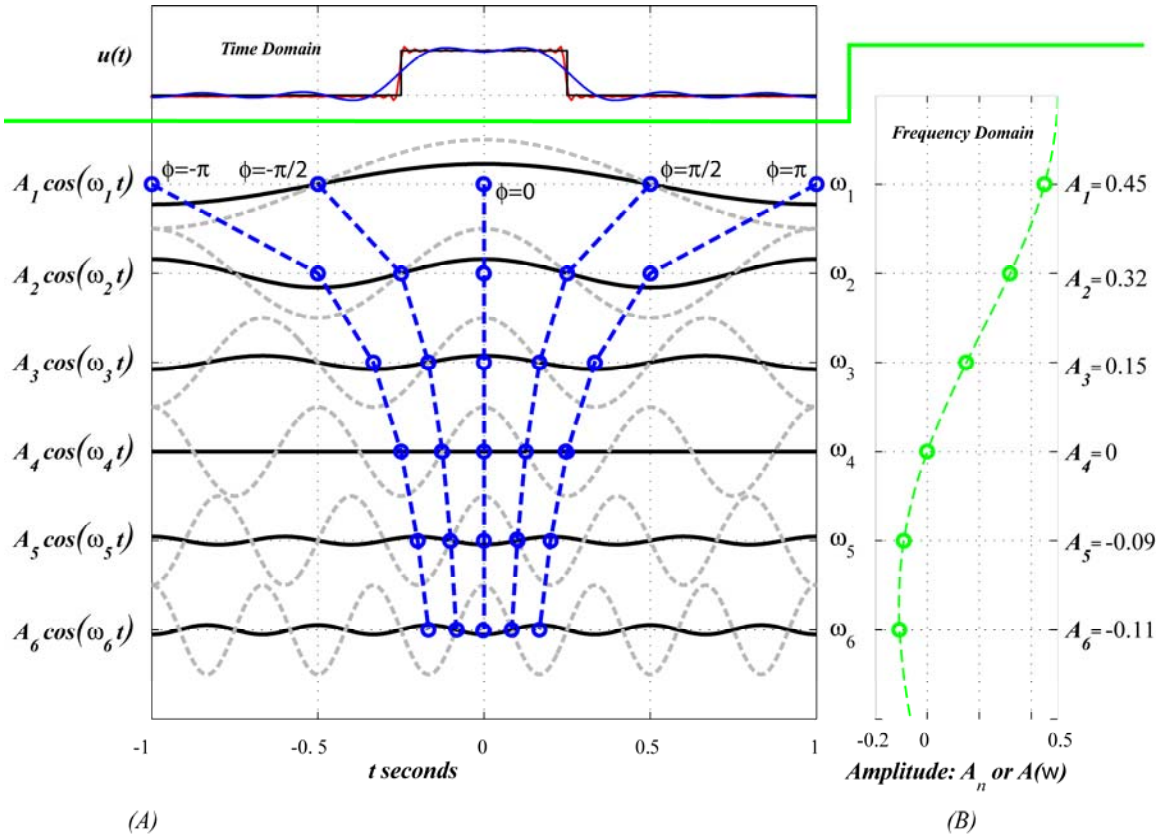

Figure 1. (A) Plots of boxcar time-domain function (top part: black) and its approximations using the first 7 terms of its Fourier series (blue) and the first 100 terms (red). The DC (zeroth) term in the Fourier series, a_0, which is weighted differently than the other terms and provides a constant y offset in the time-domain, is not plotted in either (A) or (B) but is included in the sum. Plots of the first through sixth sinusoidal basis functions (bottom part: gray dashed lines) and the corresponding terms of the Fourier series after applying the frequency-domain weights (bottom part: black lines). Several sets of points where the argument to the sinusoidal term is a constant are shown by blue circles. The blue dashed line connects these points as one goes between the terms of the Fourier series. These curves become lines of constant phase of the argument for the continuous Fourier transform integrand. The circles are drawn on the axis for each basis function, not on the plot of the function. Note the overshoots at the sides of the boxcar. This is a "feature" of the finite Fourier series, known as the Gibbs phenomena, which we will not be able to remove. The time axis is in seconds and $\omega_1 = \pi$ radians/second. (B) Weights for the Fourier series terms (green circles) and the continuous Fourier transform amplitude spectrum (green dashed line). One of the main purposes of this tutorial is to use a graphical presentation to facilitate understanding the shape of the time-domain function in terms of the Fourier transform integrand. The figures will, therefore, be scaled for the graphics presentation, rather than following the scaling rules of the forward and inverse Fourier transforms. The continuous Fourier transform weights shown above have, therefore, been rescaled to match those of the Fourier series terms. The property of the

Fourier transform and Fourier series weights that is important here is the shape of the function in the frequency-domain, not the amplitude.

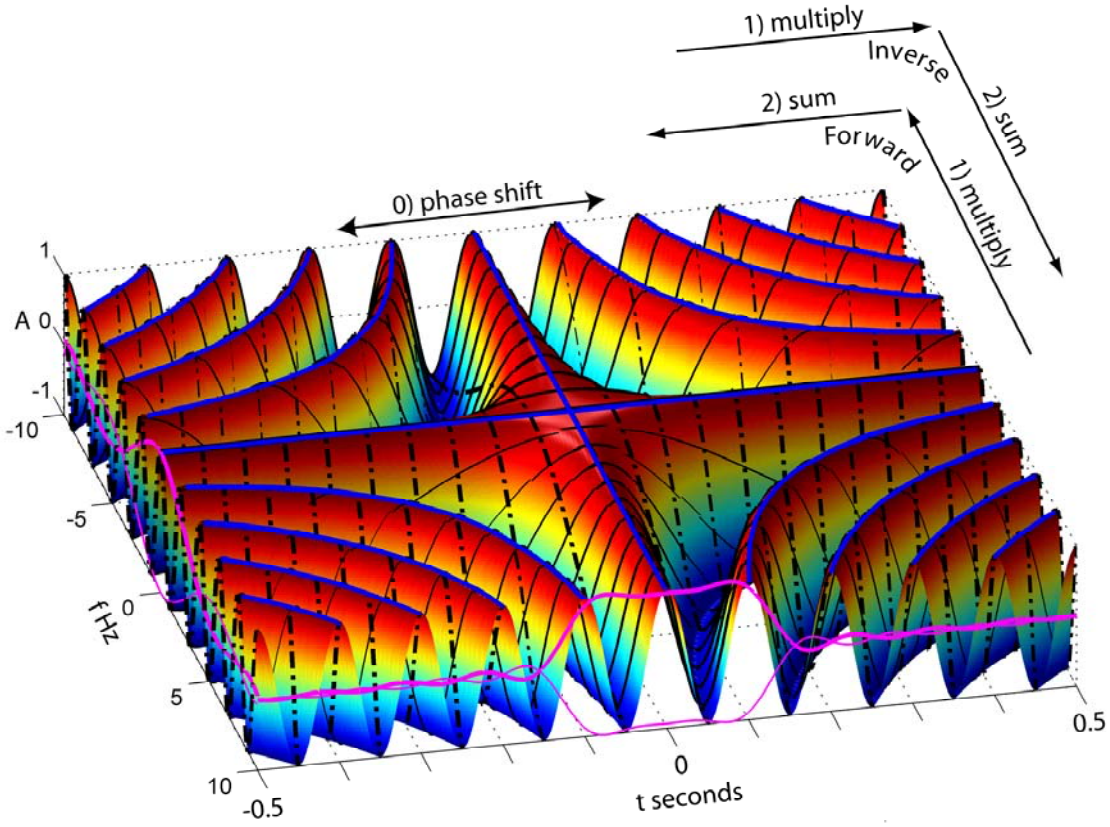

Figure 2(A). 3-D view of the set of basis functions, $\cos(\omega_n t_m)$, which is common to the integrand of both the forward and inverse continuous Fourier transforms. The time axis (*t*, right side) is in units of seconds and ranges from -0.5 to 0.5 seconds. The frequency axis (*f*, front) is in units of Hz (cycles/time unit) and ranges from 0 to 10. The vertical axis (height) is the amplitude of the Fourier component at (t,ω). Color shows the value at each point (t,ω), while the lighting and shading help the brain visualize the surface. The solid black lines parallel to the time axis are the Fourier series components shown in Figure 1a. The blue lines along the crests show lines of constant phase to the argument of the sinusoidal basis functions. This figure shows the symmetry between the forward and inverse transforms, which is made much clearer by including the negative frequencies in the FTIV space images.

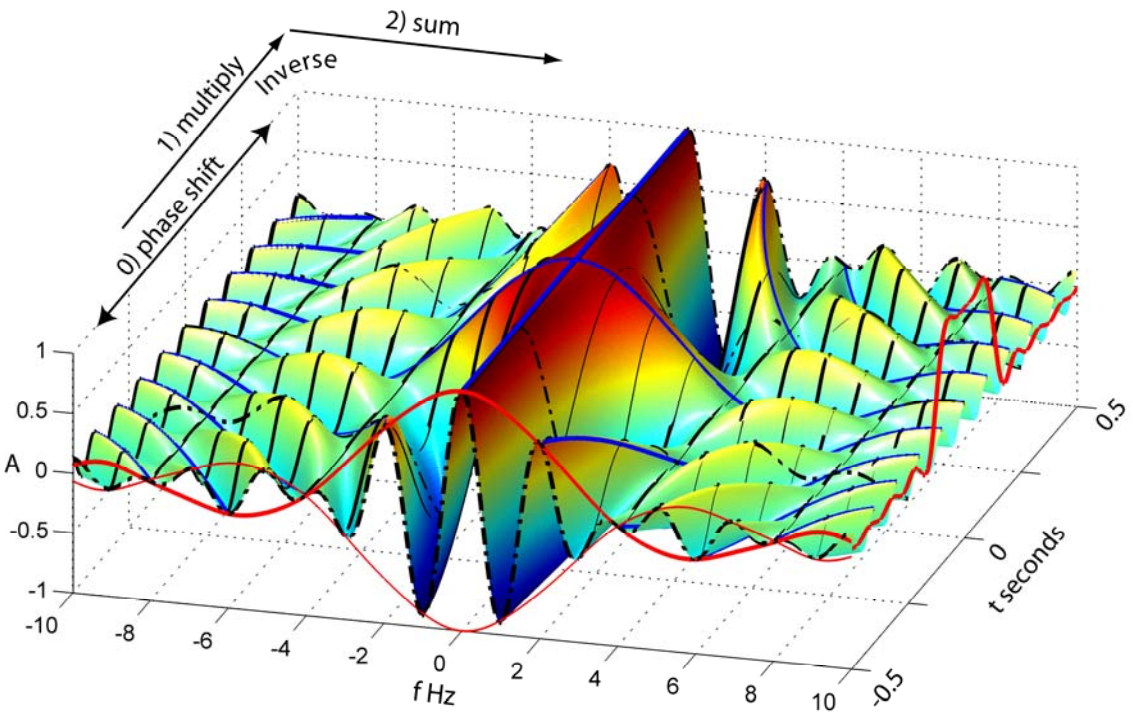

Figure 2(B). 3-D view of the integrand, $c_n \cos\left(\omega_n t_m\right)$, of the continuous inverse Fourier transform for a boxcar. The dashed black lines parallel to the frequency axis (constant time) show the function that is summed to produce the value of the time-domain function at that time. The red curve at the right is the "continuous" inverse Fourier transform. The frequency-domain function is shown along the t-axis by the heavy red curve, which together with the light red curve shows the envelope obtained after multiplying the basis functions by $F\left(\omega_m\right)$. Sums parallel to the f axis produce the red curve, $u\left(t_n\right)$, along the time axis. (Note: Both the time-domain function and the 3-D representation of the integrand are plotted normalized to their own maximum.) The frequency and time-domain functions are shown along the f- and t-axis by the heavy magenta curves, which together with the light magenta curves show the modulation envelopes of parts a and b, when the basis functions are multiplied by them.

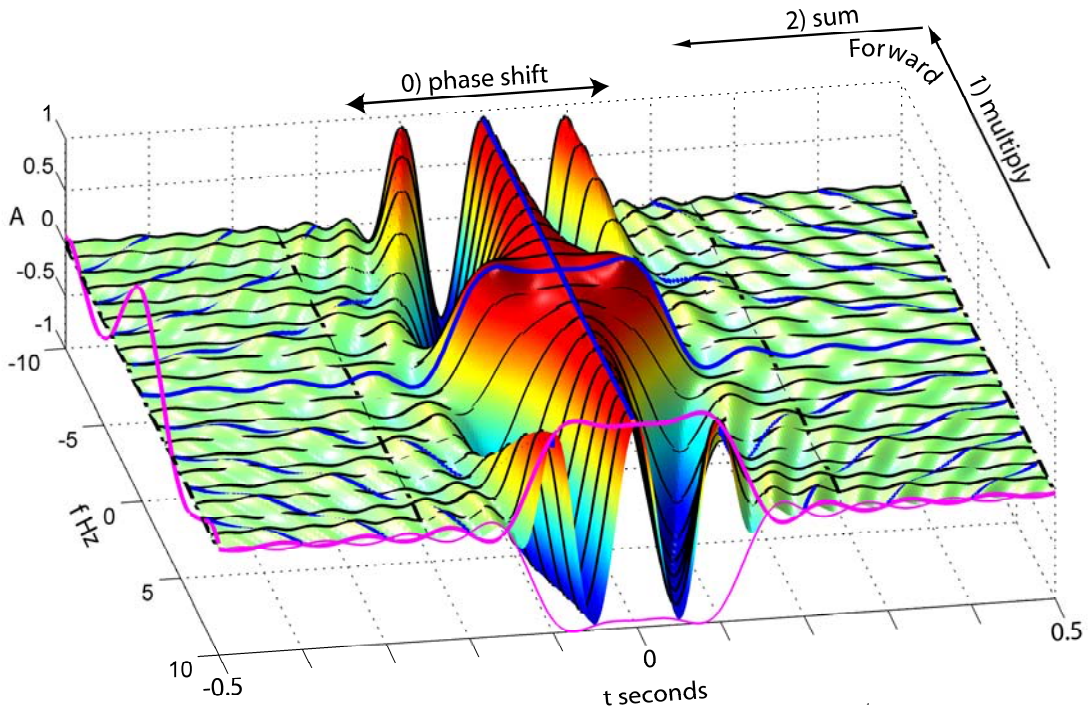

Figure 2(C). 3-D view of the integrand, $u(t_m)\cos(\omega_n t_m)$, of the continuous forward Fourier transform for a boxcar. The illumination, various lines, axes, and scaling are as in Figure 2(A). The time-domain function is shown along the x-axis by the heavy magenta curve, which together with the light magenta curve shows the envelope obtained after multiplying the basis functions by $u(t_m)$. Sums parallel to the t axis produce the Fourier transform, $F(\omega_m)$, shown by the magenta curve along the frequency axis. Note that we are now using both positive and negative frequencies in the frequency-domain and both t and ω are discrete.

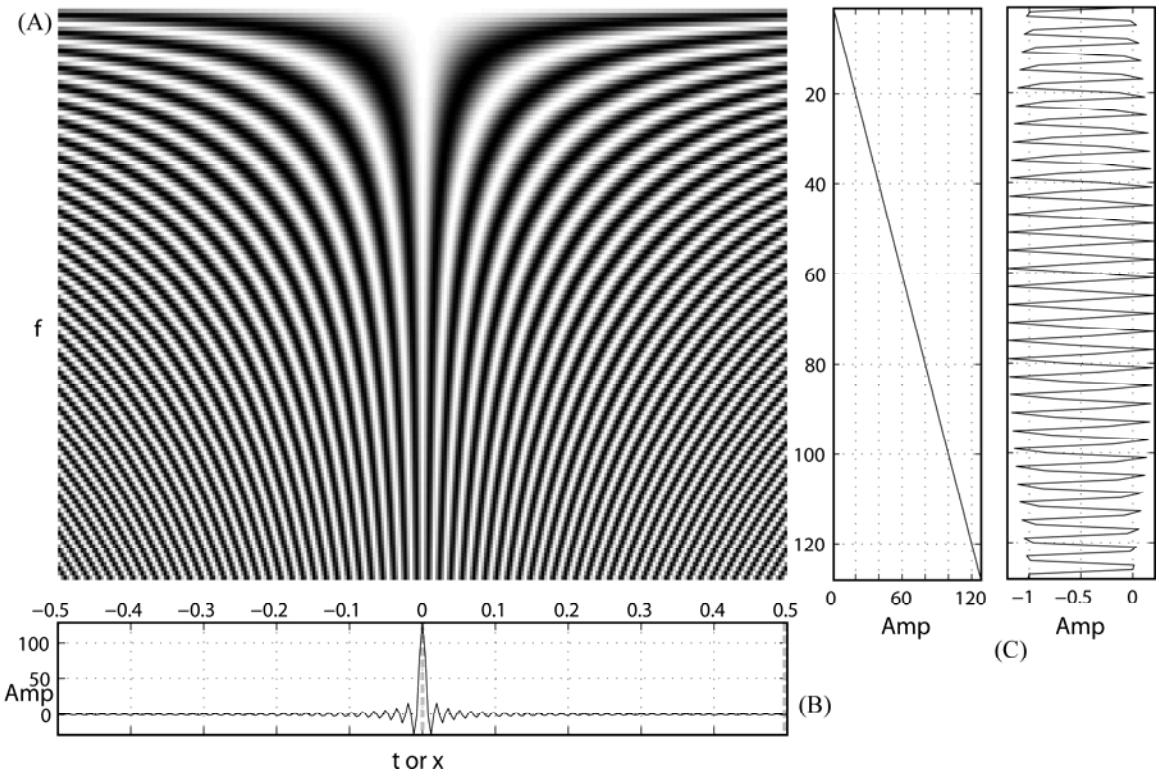

Figure 3. (A). Gray scale topographic FTIV of the inverse Fourier transform for the delta function (positive frequencies only). (B). The real-space function, calculated using the inverse Fourier transform is shown at bottom. The vertical view is similar to Figure 2a, but the "topography" is now encoded in gray, and there is no lighting or shading. (C). The plots on the right show the running sum of the inverse Fourier transform as a function of the upper frequency limit of the sum for time or position = *0* and time or position = *0.49* (grey lines). Note the very different amplitude scales on the plots of the running sum for the two positions. The horizontal axis on the bottom left is t in seconds with $\omega_1 = 2\pi$ radians/second, or x in meters and $\omega_1 = 2\pi$ radians/meter.

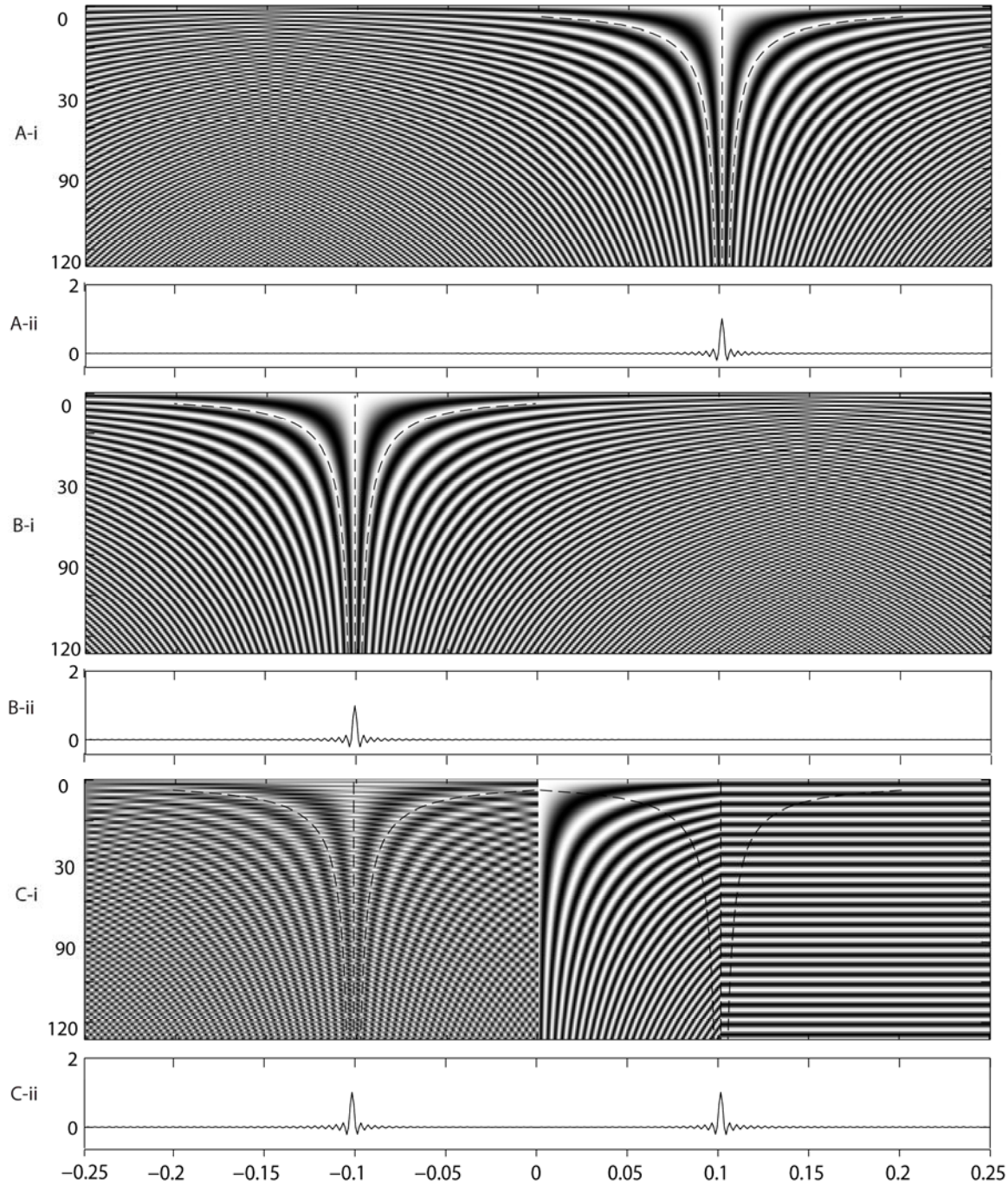

Figure 4. Combination of two traveling waves in parts (A) and (B) into standing waves in part (C). Top parts (i) show FTIV view, bottom parts (ii) show real-space function. The dashed lines in parts (A)-i and (B)-i show several lines of constant phase in the argument to the integrand. Constructive interference in parts (A) and (B) occurs only for the vertical dashed lines. The left hand side of c-i shows the full pattern produced using either the product or sum form of the combined waves in (A) and (B). The right hand

side of (C)-i shows the two components of the product form, the fixed spatial delta function, $\cos(kx)$, shown between $x = 0$ and 0.1 and the cosine modulation term, $\cos(\omega t)$, shown from $x = 0.1$ to 0.25. The time value for this snapshot is such that the two cosines match at $x = 0.1$ (under the vertical dashed line) and the vertical sum (integration over frequency) at that point is therefore non-zero. At all other places the integrand is the product of two cosines of different frequencies and the integral is zero. The lines of constant phase in the argument to the integrand from the traveling waves are also drawn in part (C)-i, where one can still see the "skirt" patterns in the left hand side, but the skirt patterns now have a modulation as one follows any vertical profile. (The light gray skirts on the left and right of parts (A)-I, (B)-I, and the left side of (C)-I are imaging artifacts of the gray scale.)

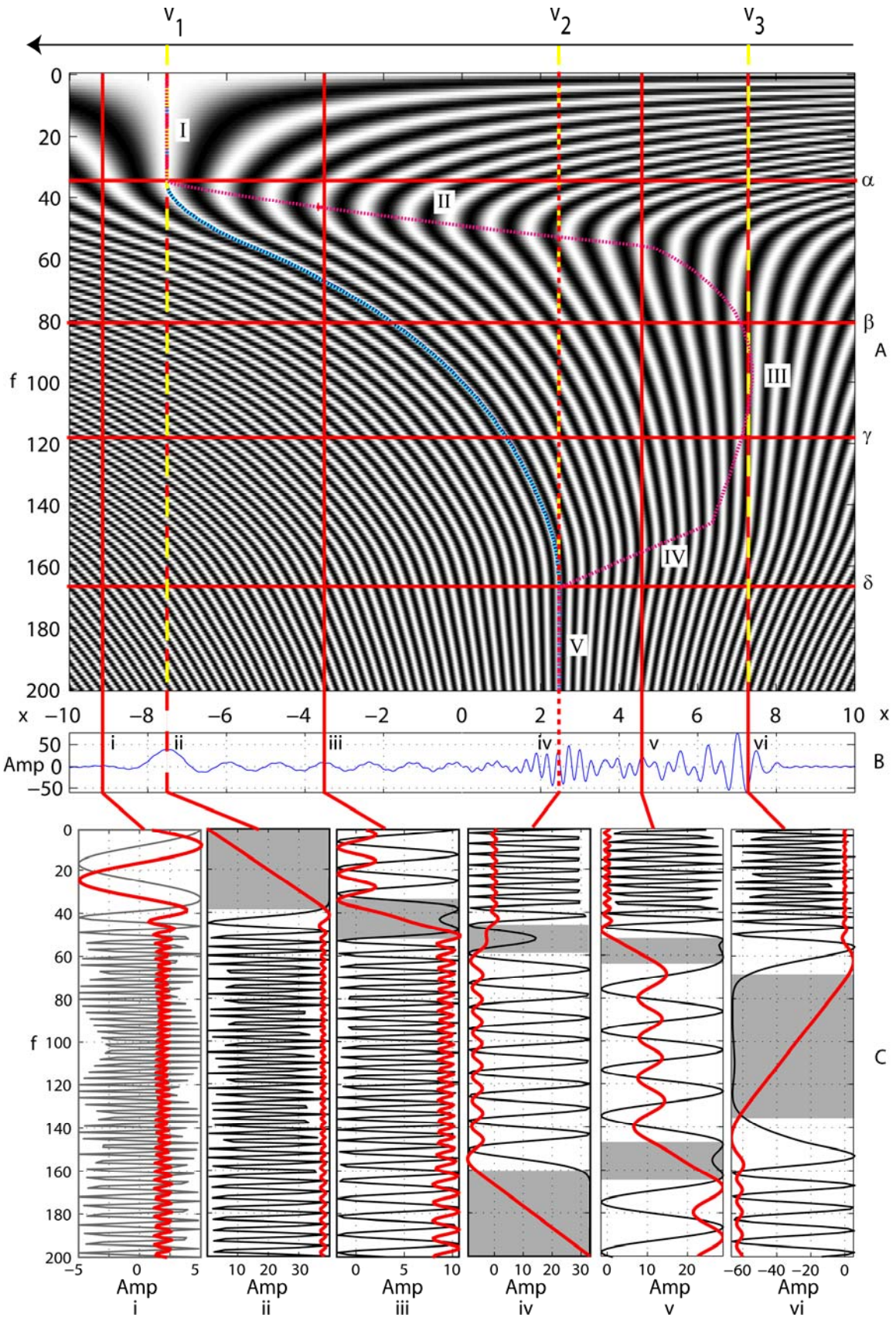

Electronic Supplement to
Student Guide: Making Waves by Visualizing Fourier Transformation by Robert Smalley, Jr.
EduQuakes column from *Seismological Research Letters* Volume 80, Number 4 July/August 2009

Figure 5. Figure illustrating dispersion, phase and group velocity, and the principle of stationary phase. Fourier integrand (A) and distance-domain (B) snapshots of a dispersed wave at time t. In the FTIV space (A) the frequency increases going down. The distance axis, shared between the FTIV space and real-space plots, is shown between the two and pans with the travelling wave such that the axis is approximately symmetric about the "center" of the dispersed wave. In (A) the phase and group velocities are shown by the cyan and magenta curves using the velocity axis across the top. Velocity increases to the left. Three velocities are marked and shown by the yellow dashed lines, the fast, v_1, and slow, v_2, limits of the phase velocity and the fast, v_1, and slow, v_3, limits of the group velocity. The four horizontal red lines, α–δ, in (A) define five branches, labeled I-V, for discussion of the group velocity and shape of the real-space wave-train. (C) Shows a selection of vertical profiles, i-vi, at different positions with plots of the FTIV function at that position, in black, and the cumulative integration, in red. The FTIV functions are all plotted on an unlabeled scale ranging from -1 to +1. The scale for each of the integrations is different and labeled on each plot. The gray regions show the regions of the integrand that contribute to the non-zero real-space waveform. In plots of the phase of the argument to the integrand (along the profiles i-vi for example) the regions of stationary phase are small and subtle and are not obvious. When the weights are equal, however, a plot of the integrand can serve as a proxy for a plot of the phase of its argument. Where the integrand looks like a single frequency harmonic wave the phase is linear (or approximately so). When the integrand looks like a harmonic wave with varying frequency, the phase is varying but not in a linear fashion. In both cases, these regions do not make non-zero contributions to the integral or sum. Finally in regions where the integrand is approximately constant (regions with gray background in i-vi), the phase of the argument to the integrand is stationary or nearly-so and significant contribution is made to the sum or integration.

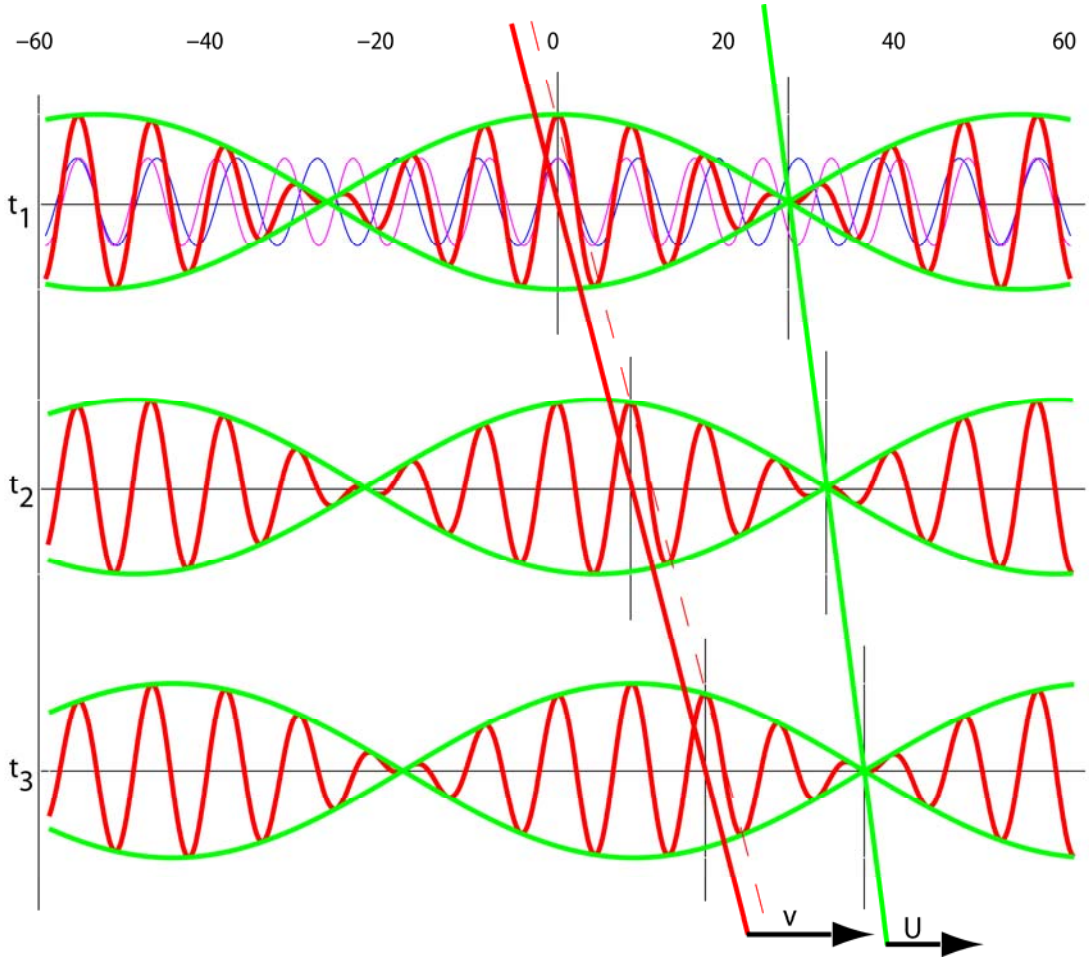

Figure 6(A). Standard figure showing relationship, and difference, between phase velocity, v, and group velocity, U. The horizontal axis is distance, so we are looking at snapshots of the wavefield. At time t_1, the individual component waves are also shown. Note that they are in phase at $x = 0$, and every maximum of the envelope, and out of phase at $x \approx 25$, and every zero of the envelope. In this case, $v > U$ and the wiggles move forward through the envelope. The red curve shows the carrier waves and the slanted red line labeled, v, shows the phase velocity. If one were to sit on a crest, one would move at this velocity. The group velocity at which the envelope moves is shown by the slanting green line.

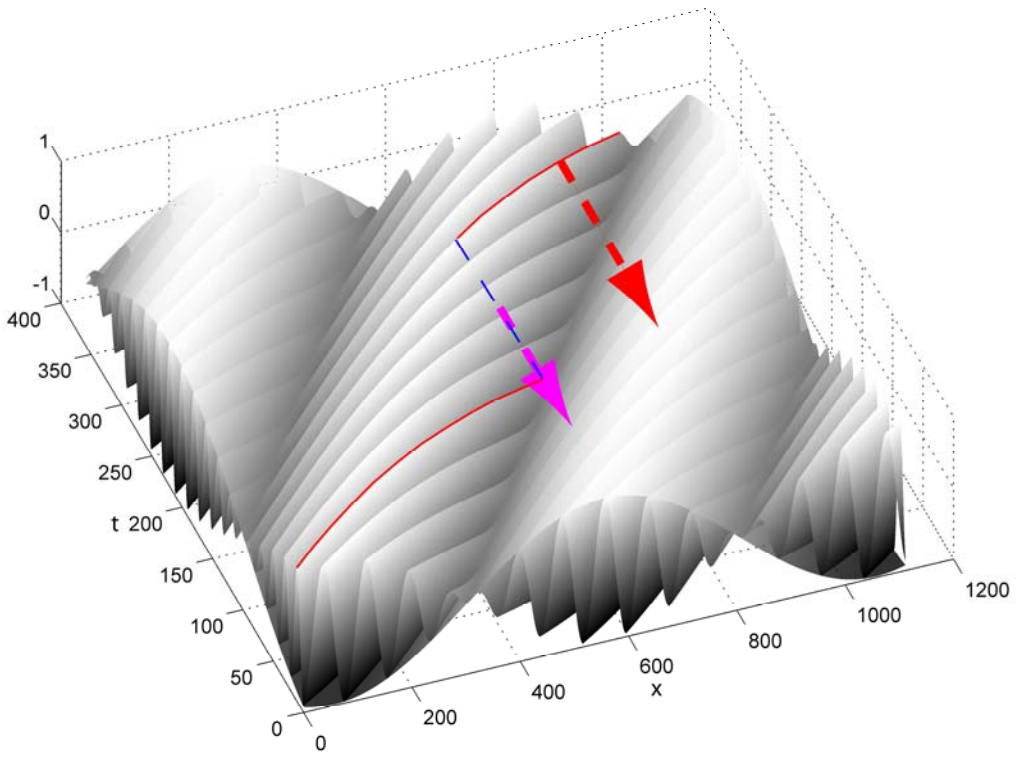

Figure 6(B). Three dimensional view illustrating phase and group velocity as a function of (x,t). The carrier is drawn as an opaque surface and one side of the envelope, is drawn over the carrier as a transparent surface. Points of constant phase argument in the carrier (a crest for example, example shown in red at right) move at the phase velocity (red vector), v, through the modulating envelope, which moves at the group velocity (magenta vector), U.

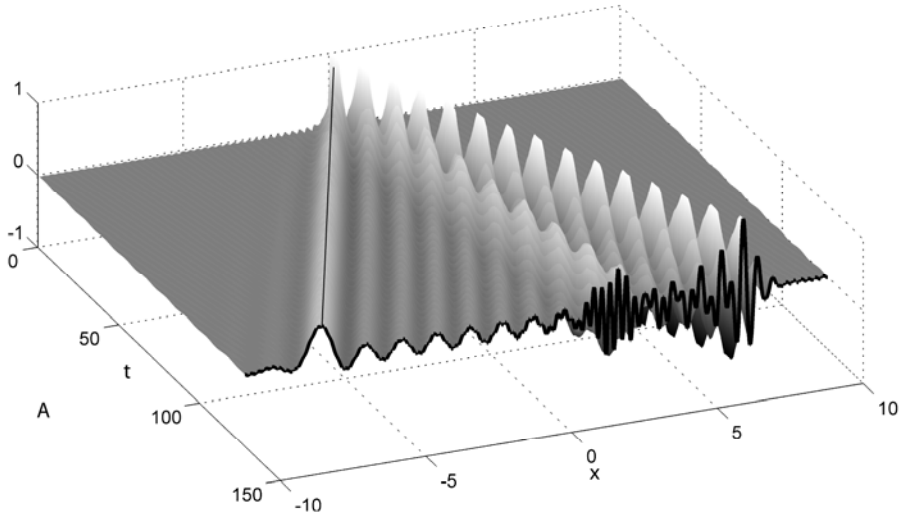

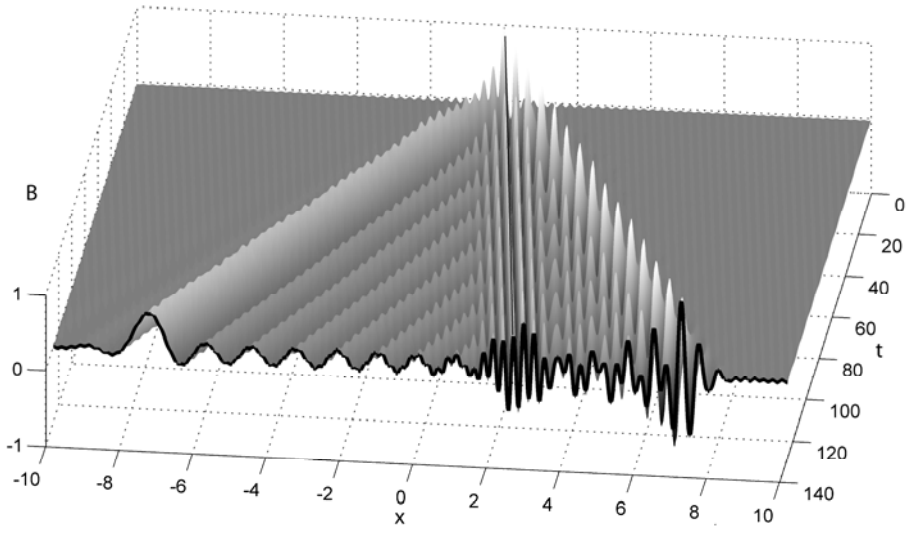

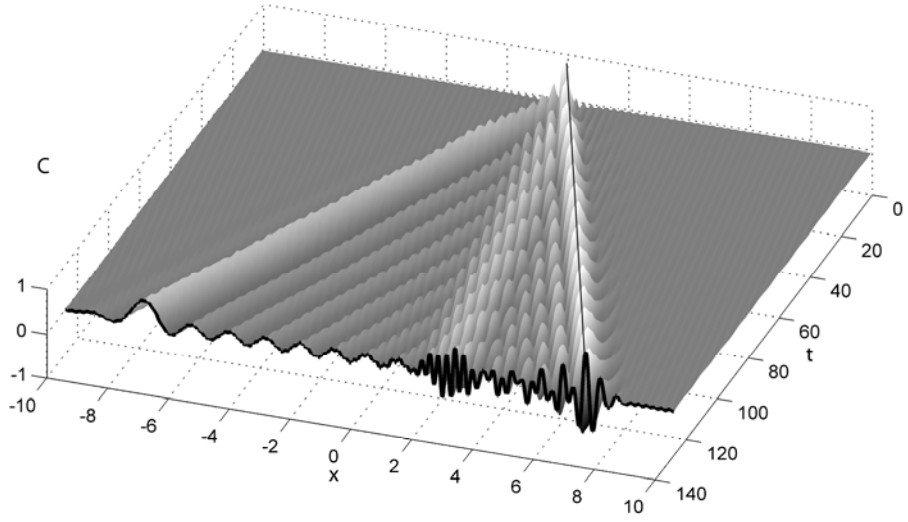

Electronic Supplement to
Student Guide: Making Waves by Visualizing Fourier Transformation by Robert Smalley, Jr.
EduQuakes column from *Seismological Research Letters* Volume 80, Number 4 July/August 2009

Figure 7. Waterfall views of the time evolution of the dispersing wavefield with a reducing velocity $v_r = (v_1 + v_3)/2$. Wavefield features that slope to the left travel faster, and those that slope to the right travel slower, than the reducing velocity. The wavefield at, t_1, is plotted in black at the front and is the same as in Figure 5. As time increases, the wavefield and therefore the energy is spread over a larger distance, and the amplitude decreases. In order to see the evolution of the shape, each wavefield trace is therefore normalized by its maximum amplitude, which occurs in the Airy phase at the back.

SEISMOLOGICAL RESEARCH LETTERS

Volume 80, Number 3 May/June 2009

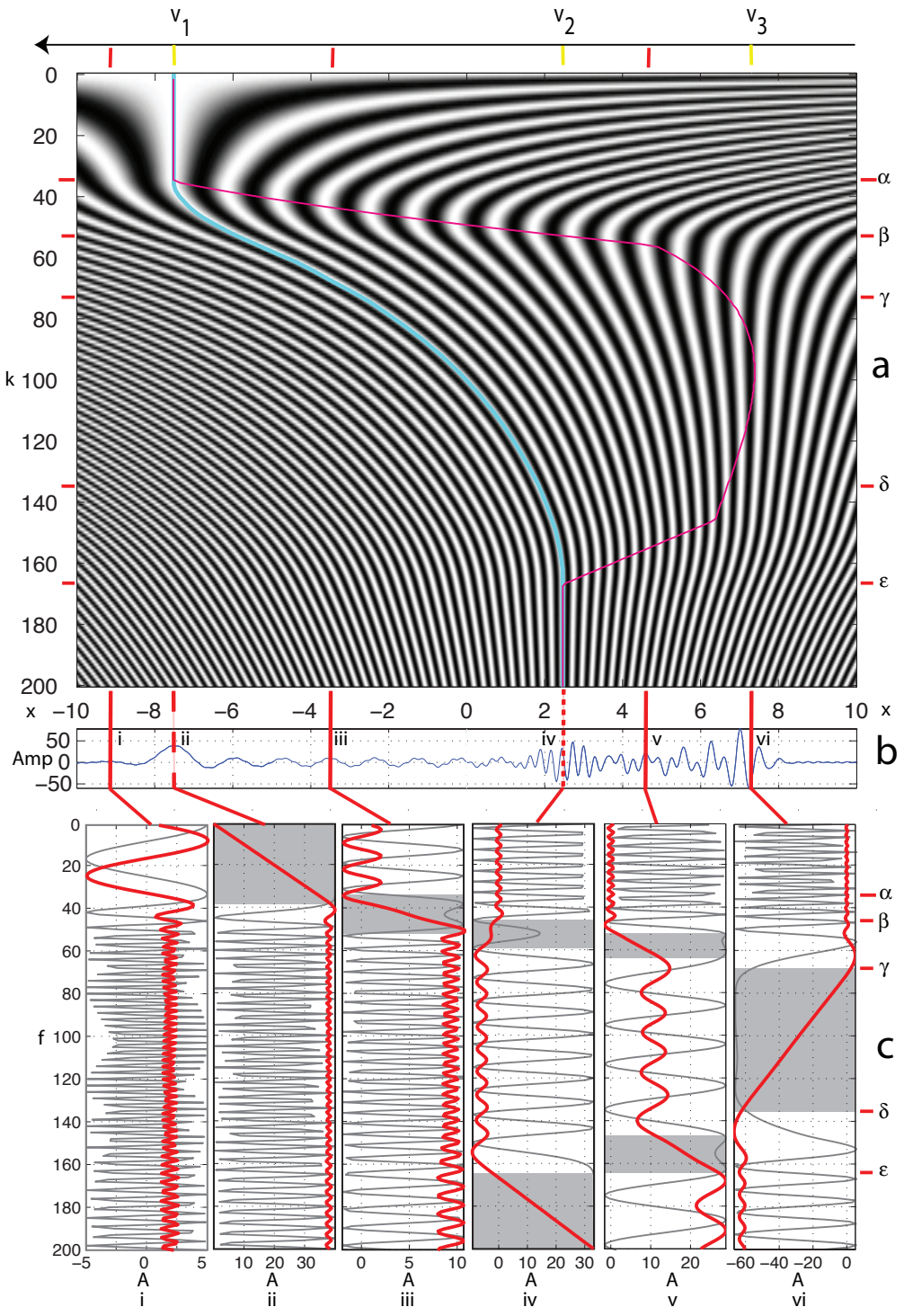

SEISMOLOGICAL SOCIETY OF AMERICA

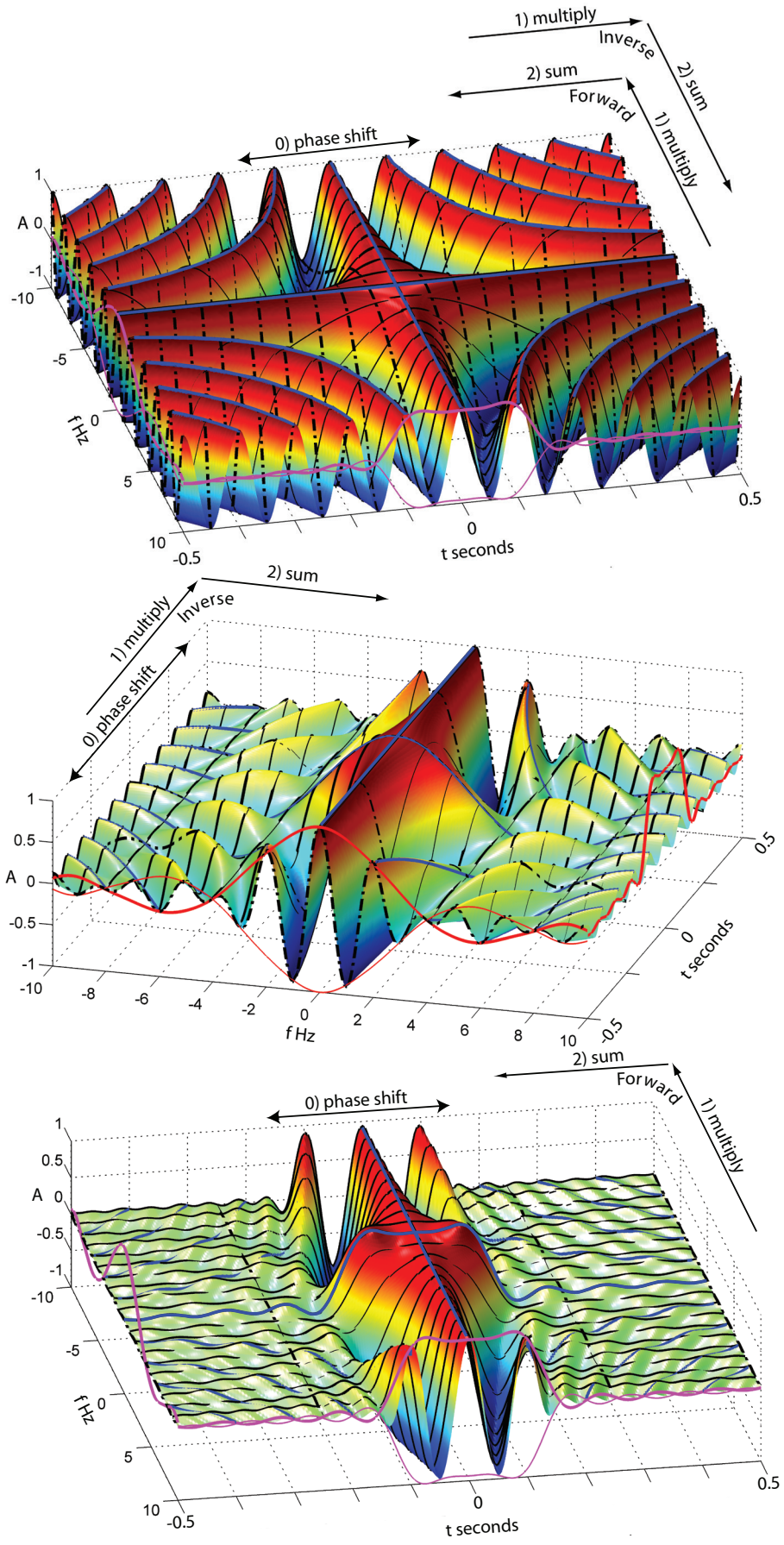

Seismological Society of America
201 Plaza Professional Building
El Cerrito, CA 94530